THE TOXICOLOGY, PHARMACOKINETICS AND METABOLISM OF A NOVEL IL-6 INDUCED STAT3 INHIBITOR

by

Brian F. Kiesel

Bachelor of Science (B.S.) University of Pittsburgh, 2009

Submitted to the Graduate Faculty of

The School of Pharmacy in partial fulfillment

of the requirements for the degree of

Master of Science

University of Pittsburgh

2016

UNIVERSITY OF PITTSBURGH

SCHOOL OF PHARMACY

This thesis was presented

by

Brian F. Kiesel

It was defended on

August 5th, 2016

and approved by

Julie L. Eiseman, Ph.D., D.A.B.T., Dept. of Pharmacology and Chemical Biology

Paul A. Johnston, Ph.D., Dept. of Pharmaceutical Sciences

Raman Venkataraman, Ph.D., Dept. of Pharmaceutical Sciences

Thesis Advisor: Jan H. Beumer, Pharm. D. Ph.D., D.A.B.T., Dept. of Pharmaceutical Sciences

THE TOXICOLOGY, PHARMACOKINETICS AND METABOLISM OF A NOVEL IL-6 INDUCED STAT3 INHIBITOR

Brian F. Kiesel

University of Pittsburgh, 2016

Head and neck squamous cell carcinoma (HNSCC) is the sixth most common cancer and annually an approximate 46,000 Americans are diagnosed and 8,600 Americans die from the disease. The oncogenic transcription factor STAT3 is frequently hyper-activated in HNSCC and promotes gene transcription involved in cancer development, maintenance and progression. Several selective small molecule inhibitors of IL-6-induced STAT3 activation were identified in a screening campaign, and four analogs from a lead optimization series were analyzed to promote one to test *in vivo*.

To choose a lead compound for *in vivo* experimentation, the four compounds were incubated with mouse liver microsomes to select a lead based on enhanced metabolic stability. From this experiment compound UPCDC-10205 was prioritized for *in vivo* testing to evaluate its toxicity, pharmacokinetics (PK) and metabolism. Both single and multiple IV dose toxicity studies determined that the maximum soluble dose at 4 mg/kg of compound UPCDC-10205 in 10% Solutol™ was not toxic to mice. To evaluate PK, single doses of UPCDC-10205 IV 4 mg/kg, PO 4 mg/kg, or PO 30 mg/kg UPCDC-10205 suspension in 1% carboxymethyl cellulose were administered to groups of female mice that were euthanized from 5 min to 24 h after dosing. Plasma, urine and various tissues were analyzed using LC-MS to quantitate UPCDC-10205. PK parameters were determined non-compartmentally. Potential metabolites were monitored in plasma and urine using LC-MS.

PK analysis showed rapid plasma clearance and extensive distribution of UPCDC-10205. Comparisons of plasma exposure between 4 mg/kg PO and IV showed a bioavailability of ~5%. Little UPCDC-10205 was observed in urine, leading to the hypothesis that metabolism was the major contributor to clearance. Metabolic investigations revealed direct glucuronidation as the

major metabolite, explaining why microsomal stability (reflective of phase I metabolism) did not translate to *in vivo* metabolic stability.

TABLE OF CONTENTS

LIST OF TABLES

LIST OF FIGURES

LIST OF EQUATIONS

1.0 INTRODUCTION

1.1 HEAD AND NECK SQUAMOUS CELL CARCINOMA

Head and neck squamous cell carcinoma (HNSCC) accounts for 90% of diagnosed head and neck cancers and originates from the epithelium of the pharynx and oral cavities.[1] The development of HNSCC has been correlated with a variety of factors, including tobacco use and human papilloma virus.[2, 3] HNSCC is the sixth most common cancer with approximately 46,000 Americans diagnosed and 8,600 Americans dying from the disease annually.[1, 4] Men account for approximately 70% of those afflicted and dying.[4] Five year survival rates for all stages of head and neck cancer are 60% with only modest improvements within the past 40 years.[1] The majority of diagnoses are of advanced stage and 60% of patients will also have recurrent or metastatic disease.[1, 5] Patients diagnosed with recurrent or metastatic HNSCC currently have no curative options.[5] The current standard of care for HNSCC varies depending on disease site and stage, but treatment usually involves combinatorial surgery and radiation.[1] Chemotherapeutic options for late stage HNSCC are considered palliative and no current therapies have demonstrated a proven benefit to survival.[1] Due to these factors, there has been an urgent and unmet need to identify new chemotherapeutic options for HNSCC and increase survival rates, especially in cases of recurrent and metastatic HNSCC.

1.2 STAT3

Signal transducer and activator of transcription 3 (STAT3) activation has been implicated in most cancer types including HNSCC.[1, 6-10] STAT3 has been found to be constitutively active in HNSCC cell lines and tumors.[6, 10] Identification of this biomarker and elucidation of its contributions to carcinogenesis may help to identify new therapies to combat the disease.[1, 9] STAT3 has also been used as a prognostic factor for staging the disease, with increased STAT3 activation translating to a poorer clinical outcome.[8] Aberrant STAT3 activation can lead to the initiation, development and metastasis of cancers by misregulating the genes and proteins needed to overcome cancer progression barriers.[6, 7, 9, 11, 12] As well as directly manipulating gene expression, STAT3 has been found to alter expression non-directly by epigenetic DNA methylation.[13] STAT3 has also been shown to play a role in chemoradiotherapy resistance.[14] Understanding the STAT3 pathway and its involvement in cancer pathophysiology may help researchers and clinicians modulate its effects in cancer and other diseases.

1.2.1 STAT3 Pathway

STAT3 is part of a seven member protein family that act as cytosolic signal transducers and transcription factors that regulate gene transcription.[6, 8, 9, 15] STAT members are structurally similar and have overlap in gene transcription, although each has unique targets of transcription.[6, 8] STAT transcriptional activation requires phosphorylation on a single tyrosine residue towards its carboxyl terminus (Tyr705).[6-9, 15] This phosphorylation is usually initiated in response to upstream cytokines or growth factors that activate their respective receptor or associated kinases which are then able to directly phosphorylate specific STAT family

members.[6, 8, 15] Upon phosphorylation by an upstream kinase, STAT proteins dimerize and translocate to the nucleus where they can act as transcription factors by binding to promoter regions of their regulated genes.[6, 8, 16] **Figure 1** shows a simplified STAT3 activation pathway.

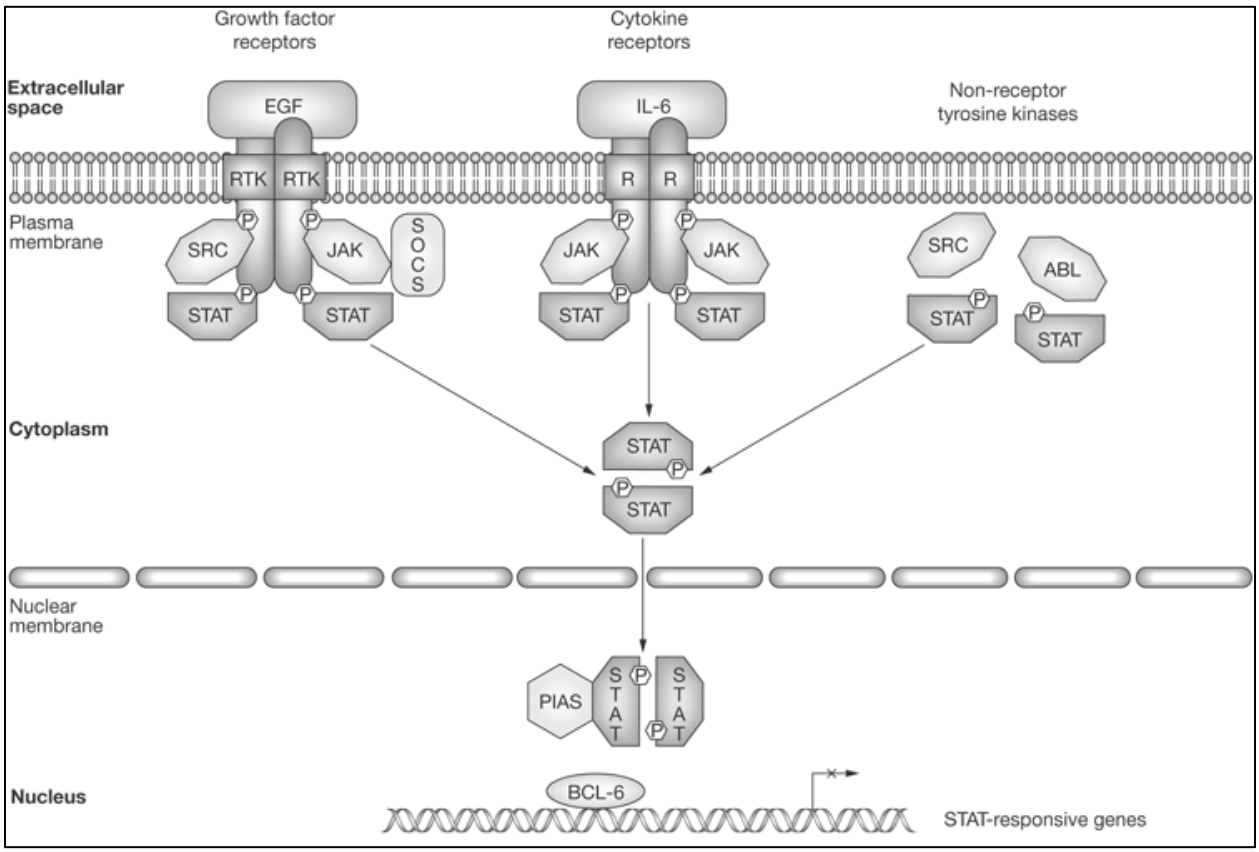

Figure 1. Schematic representation of STAT signaling pathways.[17]

1.2.2 STAT3's Role in Cancer

Within the STAT family, STAT3 has been found to regulate functions such as cellular proliferation, cell cycle progression, apoptosis, angiogenesis, immune invasion, survival, inflammation, invasion and metastasis.[6-8, 11, 16, 18] In non-disease states, interleukin-6 (IL-6) induced STAT3 activation is used to provide survival cues and block apoptosis during inflammatory processes.[19] Cancer development can hijack the IL-6/STAT3 signaling pathway to

constitutively activate STAT3 and promote carcinogenesis. In cancer cells, STAT3 has also been shown to silence its negative regulator, SOCS (suppressor of cytokine signaling).[8] The link between constitutively activated STAT3 signaling and cancer earned STAT3 the label of oncogene.[6, 7] STAT3's role as a point of convergence for multiple cancerous pathways has made it an attractive target for the development of new chemotherapeutic therapies.

EGF/EGFR and IL-6/IL-6R have been identified as primary, but not the only, regulators of STAT3 phosphorylation and treatments that target these pathways are currently being pursued.[6, 7, 13] EGFR modulating chemotherapies have become promising agents for HNSCC but so far drugs targeting EGFR signaling have been found to only offer disease control and offer palliative care, with no tumor regression in HNSCC.[1, 7] Additionally, evidence has shown that eventual drug resistance is developed against EGFR inhibitors.[5, 7] One reason for resistance is that there are multiple pathways that lead to STAT3 activation besides EGFR, suggesting that other STAT3 activators, such as IL-6, should be targeted for STAT3 modulation.[5] A growing body of evidence has implicated IL-6 production in HNSCC cells as the predominant activator of STAT3.[10] Investigations of STAT3 activation in HNSCC cell lines have shown that even in EGFR-positive lines, STAT3 activation is not dependent on EGFR activation.[10] Subsequently, depletion of IL-6, blocking the IL-6R subunit (gp130) or the IL-6R associated intracellular kinase (Janus kinase of JAK), leads to decreased activated STAT3 (pSTAT3).[6, 10] This research implicates IL-6 is the primary factor for STAT3 activation in HNSCC.[10] Clinically, both increased IL-6 and pSTAT3 levels have been associated with a poorer prognosis for those with cancer.[8, 13] Serum IL-6 levels have also been used to predict HNSCC patient survival.[20-22]

1.2.3 STAT3 as a Target

Targeting IL-6 induced STAT3 activation in HNSCC has been a logical target to develop therapies. IL-6 has been described as the traditional activator of STAT3.[13] Canonical IL-6 signaling pathway requires IL-6 to bind to its receptor, IL-6Rα.[13, 23] This interaction causes the recruitment of gp130 subunits to the ligand-receptor complex.[13, 23] Two of these complexes interact together to form a hexamer that in turn causes intracellular autophosphorylation of JAKs.[13, 23] Activated JAKs are able to phosphorylate STAT3 proteins on their tyr-705 residue.[23] Two phosphorylated STAT3 proteins then homodimerize, which allows for the translocation of the dimer into the nucleus where it can act as a transcription factor.[13, 23]

Despite the growing amount of literature that implicates STAT3 in cancer development and progression, there are currently no approved therapies that directly target STAT3.[13] Several strategies to inhibit IL-6 induced pSTAT3 in HNSCC have been evaluated, with each targeting specific parts of the signaling cascade. STAT3 decoy oligonucleotides have been developed that act by binding pSTAT3 in the cytosol and inhibit its function as a transcription factor.[24] Another strategy is the use of IL-6R monoclonal antibodies, which are currently being used clinically to treat rheumatoid arthritis.[25] Many small molecule inhibitors of pSTAT3 have been identified and are in various phases of preclinical and clinical development.[9, 26] Some, such as OPB-31121, have clinically demonstrated antitumor activity.[27]

One consideration when targeting IL-6 induced pSTAT3 inhibition is specificity. Due to the structural homology of STAT family members (Figure 2), a drug targeting STAT3 should be selective and not interfere with functions of other STAT members, particularly STAT1 which acts a tumor suppressor.[8, 28]

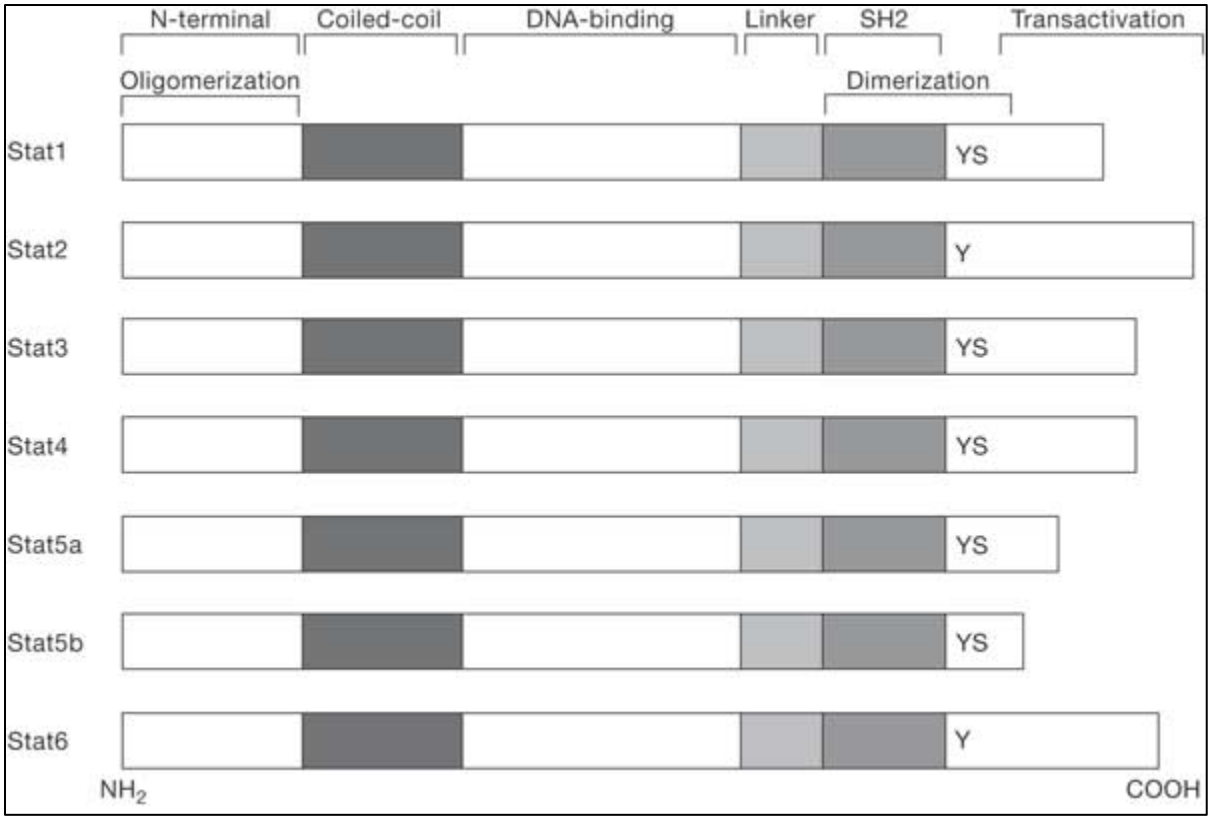

Figure 2. Structures of STAT family members.[17]

STAT1 is the singular downstream target of interferon-γ (IFN-γ) signaling.[8] Many of the genes it promotes are antagonistic to those of STAT3.[28, 29] STAT1 provides anti-proliferative, pro-apoptotic, and immune system recruitment and in its own right could serve as a therapeutic target.[28, 30]

STAT1 phosphorylation, similar to STAT3, is accomplished through intracellular JAKs that are activated by IFN-γ binding to its cognate receptor.[31] Due to the overlap in utilization of JAKs and the structural homology between STAT1 and STAT3, an ideal small molecule inhibitor of pSTAT3 should demonstrate specificity to preserve the tumor suppressive function of STAT1.[15, 16, 30] Targeting IL-6 induced STAT3 activation may lead to less off-target effects,

especially in HNSCC, where elevated levels of IL-6 are present in the local tumor environment, and prevent suppression of STAT1 signaling.[20]

1.3 CAMPAIGN TO IDENTIFY AN IL-6 INDUCED STAT3 INHIBITOR

Recently, a high content screen was developed and validated using HNSCC cell lines to identify novel small molecule inhibitors of IL-6 induced pSTAT3.[32] This screen identified 1,068 active hits from a 94,491 compound library. Active hits from the screen were confirmed with pSTAT3 IC_{50} assays and prioritized using an assay quantifying IFN-γ induced pSTAT1 activation.[33] Forty-nine compounds met the following selection criteria: reproducibly inhibiting IL-6-induced pSTAT3 activation by at least 70% at 20 μM; pSTAT3 activation IC_{50}s less than 25 μM; and at least 2-fold selective for pSTAT3 inhibition over pSTAT1 inhibition.[33] From the forty-nine compounds, a group of four triazolothiadiazine analogues (Figure 3), named the 669 series, were chosen for *in vivo* consideration based on chemical tractability and favorable *in silico* ADME-Tox attributes.[33]

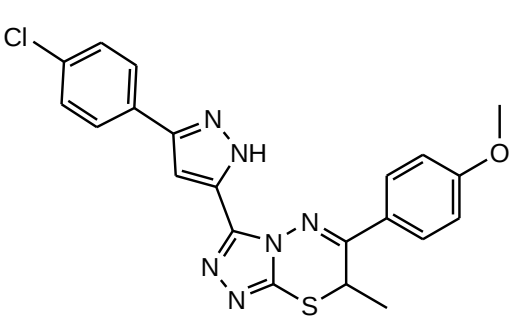

UPCDC-10205

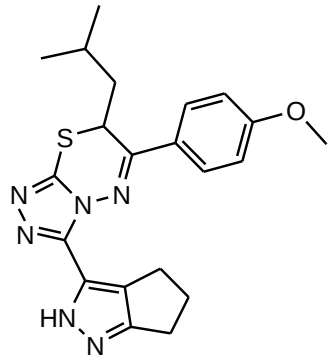

UPCDC-10305

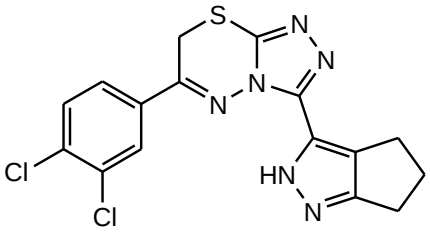

864669

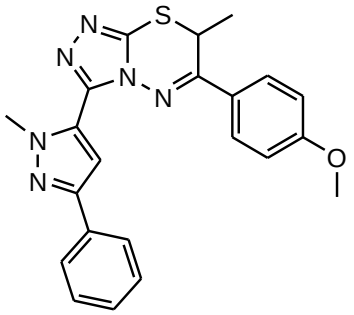

UPCDC-10540

Figure 3. Structures for the selected four IL-6 induced STAT3 inhibitor analogues from the 669 series.

To identify a lead candidate for *in vivo* examination among the four analogues in the 669 series, a mouse liver microsome incubation was conducted to identify the most metabolically stable compound of the series. It is common practice to prioritize a lead candidate using *in vitro* techniques, such as cyp P450 screens, to prioritize for metabolic stability because metabolism can directly affect toxicity, bioavailability, and clearance.[34, 35] To prioritize an analogue by metabolic stability, a microsome incubation experiment was used to assess which analogue had the most parent compound remaining after a 90 min incubation. Compound concentrations were monitored for this determination using LC-MS. The prioritized compound was then examined *in vivo* by conducting toxicity and pharmacokinetic (PK) studies. Toxicity was assessed in separate

single and multiple dose studies to determine acute toxicity as well as establishment of a maximum tolerable dose (MTD). The PK study examined intravenous (IV) and oral (PO) administration of the compound in solution (10% Solutol™ HS15) as well as PO administration with a 1% carboxymethyl cellulose (CMC) suspension. Compound concentrations were measured in plasma and tissues using a sensitive LC-MS/MS assay to determine PK parameters and bioavailability. Using LC-MS, the metabolic fate of the compound was determined *in vivo* and the biotransformation confirmed by replicating it *in vitro*.

2.0 MATERIALS AND METHODS

2.1 CHEMICALS AND SOLVENTS

Compounds UPCDC-10205, UPCDC-10305, 864669, and UPCDC-10540 were synthesized and provided by the University of Pittsburgh Chemical Diversity Center (Pittsburgh, PA). The internal standard $^{2}H_{7}$-UPCDC-10205 ([$^{2}H_{7}$]-3-(3-(4-chlorophenyl)-1H-pyrazole-5-yl)-6-(4-methoxyphenyl)-7-methyl-7H-[1,2,4]triazolo[3,4-b][1,3,4]thiadiazine) was custom synthesized and purchased from ALSACHIM (Illkirch-Graffenstaden, France). Water and acetonitrile (both HPLC grade), formic acid, monobasic and dibasic KPO4, tris and DMSO were obtained through Fisher Scientific (Fairlawn, NJ). Bovine serum albumin (BSA), NADPH, carboxymethyl cellulose (suspending agent), UDPGA, $MgCl_2$, alamethicin, formic acid and Solutol™ HS 15 were purchased from Sigma-Aldrich (St. Louis, MO).

2.2 SELECTION OF *IN VIVO* CANDIDATE

2.2.1 Preparation of Mouse Tissue Homogenates and Hepatic Fractions and Incubation with STAT3 Inhibitors

Microsomes were prepared and isolated from livers of heterozygous athymic Nude-*Foxn1*^{nu}/*Foxn1*$^{+}$ female mice as previously published.[36] The microsomal pellet was stored at -80 °C until measurement of protein concentration using a protein assay kit from BioRad (Hercules, CA) with BSA as the standard. Absorbance readings were recorded at 630 nm using an Infinite M100 Pro plate reader from Tecan (Männedorf, Switzerland). Actual incubation volumes were adapted from the published method to allow for a 200 µL incubation volume.

The 200 µL incubation contained 0.5 mg/mL microsomal protein, 1,000 ng/mL drug concentration, 1 µM NADPH, 0.1 M phosphate buffer (pH 7.4) and less than 0.1% acetontrile. The incubation was terminated with 1.0 mL acetonitrile. Sample times (point of organic reaction termination) were performed in triplicate at 0 (acetonitrile added prior to addition of microsomes), 15, 30, 45, 60 and 90 min. LMP400 (0 and 90 min incubations) was used as a positive control. Respective internal standard (10 µL of 1.0 µg/mL) of either UPCDC-10540 or UPCDC-10205 was added to samples, followed by briefly vortexing and storage at -80 °C until LC-MS analysis.

2.2.2 Microsome Incubation LC-MS

An LC-MS method was developed to simultaneously quantitate the four STAT3 inhibitor analogues. Two separate MS methods (using identical LC-MS conditions) were utilized.

Compound UPCDC-10540 was used as an internal standard to quantitate compounds 864669, UPCDC-10305 and UPCDC-10205. Compound UPCDC-10205 was used as an internal standard to quantitate compound UPCDC-10540.

The HPLC method consisted of an Agilent 1100 autosampler and Agilent 1100 binary pump (Agilent Technologies, Palo Alto, CA) using a Synergi Hydro-RP 80A (4 µm particle size, 2 mm x 100 mm) column at ambient temperature. Mobile phase solvent A was 0.1% formic acid (*v/v*) in acetonitrile, and mobile phase solvent B was 0.1% formic acid (*v/v*) in water. The initial mobile phase was composed of 55% solvent A pumped at 0.3 mL/min for 5.0 min, changed to 99% solvent A and was held there for 1.0 min. At 6.1 min the percentage of solvent A returned to initial conditions of 55% for 4 min followed by injection of the next sample. Total run time was 10 min. Retention times were as follows: 3.4 min for 864669, 4.6 min for UPCDC-10205, 4.2 min for UPCDC-10305, and 4.9 min for 540 and a representative chromatogram in Figure 4. A Quattro Micro mass spectrometer (Waters Corporation, Milford, MA) was used in positive-ion SRM mode (4.0 kV capillary voltage, 40V cone voltage) to monitor *m/z* 391.0 for 864669, *m/z* 409.0 for UPCDC-10305, *m/z* 437.0 for UPCDC-10205, and *m/z* 416.0 for UPCDC-10540.

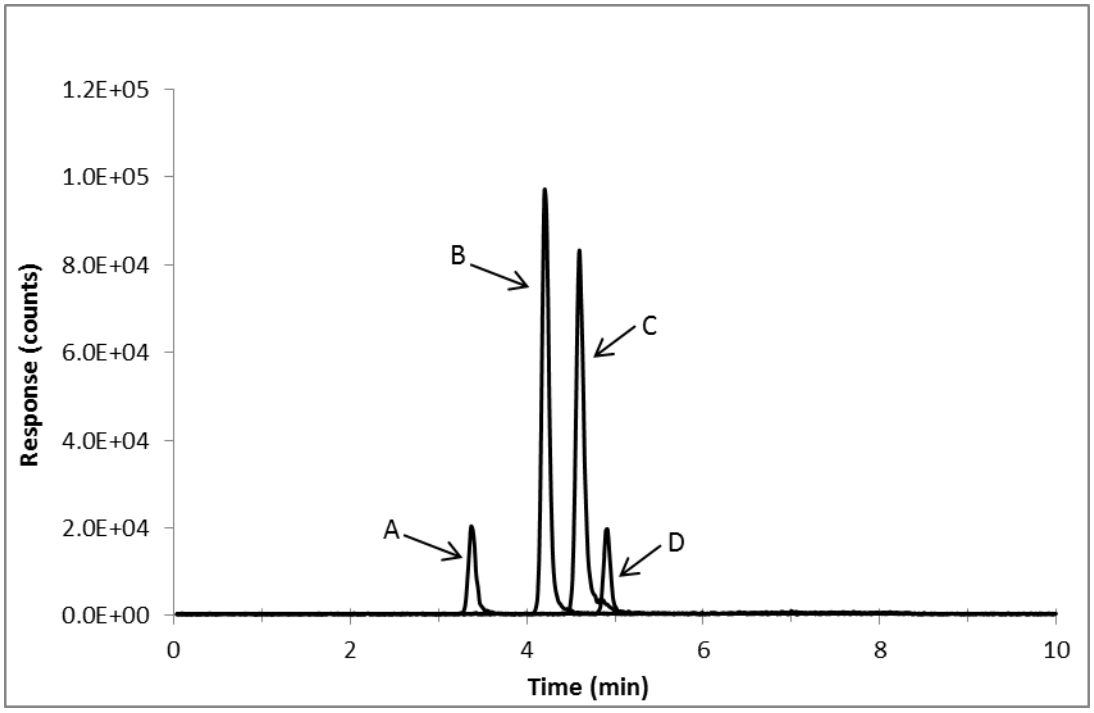

Figure 4. Representative chromatogram of a 500 ng/mL calibrator from the LC-MS assay to quantitate the selected 669 series analogues for the microsome incubation. Peak A is 864669, B is UPCDC-10305, C is UPCDC-10205, and D is UPCDC-10540.

2.2.3 Microsome Incubation LC-MS/MS Sample Preparation

Calibrators (30, 100, 300, 500, and 1000 ng/mL) were made in a 0.1M phosphate buffer (pH 7.4) that contained 0.5 mg/mL BSA to match the protein concentration of the microsomes incubation samples. A volume of 0.2 mL of the buffer mixture was placed into a 1.5 mL microcentrifuge tube. An internal standard solution (10 µL of 10 µg/mL) was added to each tube before being briefly vortexed. A volume of 1.0 mL of acetonitrile was then added and the samples vortexed for 1 minute. Samples were then centrifuged at 14,000 x g for 4 min. The dried supernatant was resuspended in 100 µL of starting condition mobile phase. The sample injection volume was 5 µL. A triplicate standard curve was prepared and analyzed for accuracy (expressed as bias) and precision prior to sample analysis.

2.3 TOXICITY STUDIES

2.3.1 Mice

Mice were specific pathogen-free, heterozygous *Foxn1*^{nu}/*Foxn1*$^{+}$ mice (50, 5-7 weeks of age) purchased from Envigo (Indianapolis, IN, USA). Mice were allowed to acclimate to the University of Pittsburgh Animal Facility for at least 1 week before studies were initiated. To minimize exogenous infection, mice were maintained in microisolator cages and handled in accordance with the Guide for the Care and Use of Laboratory Animals (National Research Council, 2011) and on a protocol approved by the University of Pittsburgh IACUC. Ventilation and airflow in the animal facility was set to 12 changes/h. Room temperature was regulated at 72 ± 4 °F and the rooms were kept on automatic 12-h light/dark cycles. The mice received Prolab ISOPRO RMH 3000, Irradiated Lab Diet (PMI Nutrition International, Brentwood, MO) and water ad libitium. Mice were fasted overnight prior to administration of UPCDC-10205. Mice were stratified based on body weights into time point groups to eliminate statistical differences in body weight. Mice were euthanized by CO_2.

2.3.2 Dosing

The vehicle 10% Solutol™ HS15 in sterile water provided the maximum solubilized concentration of UPCDC-10205 at 0.4 mg/mL and was administered to mice at a volume of 0.01 ml/g body weight as was the vehicle (10% Solutol™ in sterile water). Mice were dosed IV at 4 mg/kg using this solution for toxicity studies. This formulation was also delivered IV or PO for the PK study. A second UPCDC-10205 PO formulation was used for the PK study using 30

mg/kg carboxymethyl cellulose (CMC) suspension. Other formulations could not increase the maximum soluble dose. Dosing was accomplished for IV using ½ cc syringes with 27 gauge low dead volume needles and PO using 20 gauge 1½ inch feeding needles and 1 cc syringes.

2.3.3 Single Dose Toxicity Study

A single dose of UPCDC-10205 (at a total dose of 4 mg/kg, 0.01 ml/g body weight) was administered to both male and female mice (5 per group) IV by lateral tail vein injection along with mice administered a vehicle control. The 4 mg/kg UPCDC-10205 was formulated in water with 10% Solutol™ HS. After the single dose, mice were observed for a 14 day period to monitor clinical health, and body weights were recorded twice weekly. After the observation period, necropsies were performed on the mice to identify gross pathologies.

2.3.4 Multiple Dose Toxicity Study

For the multiple dose toxicity study, 5 female mice per treatment group were administered UPCDC-10205 daily (diluted to a total injection volume of 0.01 ml/g body weight) for 5 days IV by lateral tail vein in addition to mice administered a vehicle control. UPCDC-10205 doses used were the single dose MTD (4 mg/kg), 2/3 the single dose MTD (2.7 mg/kg) and 1/3 the single dose MTD (1.3 mg/kg). All doses were formulated to have 10% Solutol™. After the 5 day treatment, mice were observed for a 14 day period where clinical health was checked daily and body weights were measured twice weekly. After the observation period, mice were euthanized and necropsies performed on mice to identify gross pathologies.

2.4 PHARMACOKINETICS

2.4.1 Mice, Sampling, and Tissue Preparation

For the PK study, 3 female mice per treatment group per time point (5, 15, 30, 60, 120, 240, 360, 1440 min) were administered a single dose of 4.0 mg/kg UPCDC-10205 in 10% Solutol™ HS by either lateral tail vain IV injection or PO administration by oral gavage. Control mice were delivered vehicle and euthanized at 5 and 1440 min. At the appropriate time point, mice were euthanized through CO_2 asphyxiation and the following tissues collected: blood, liver, kidney, spleen, lung, heart, fat, skeletal muscle, and brain. Blood was collected through cardiac puncture in EDTA anticoagulated 22 gauge 1½ inch needles and 3 cc syringes, transferred to eppendorfs and centrifuged at 12,000xg for 3 min to separate plasma and red blood cells (RBCs). Urine and feces were from the 1440 min mice were collected from 0-360 and 360-1440 min group by housing in metabolic cages. Tissues were weighed and all samples were flash frozen using liquid nitrogen and stored at -80 °C until analysis. Necropsies were performed on all mice after euthanasia to identify gross pathologies.

2.4.2 Quantitative LC-MS/MS Assay

To support the PK study, a sensitive LC-MS/MS assay was developed to quantitate UPCDC-10205. A stable isotope, deuterated, $^{2}H_{7}$ -UPCDC-10205, was used as the internal standard. The HPLC method utilized an Agilent 1100 binary pump and 1200 series autosampler (Santa Clara, CA). Chromatographic separation was achieved using a Phenomenex (Torrance, CA) Synergi Hydro-RP 80A column (4 µm particle size, 2 mm x 100 mm) at ambient temperature. Mobile phase solvent A was 0.1% formic acid (*v/v*) in acetonitrile, and mobile

phase solvent B was 0.1% formic acid (*v/v*) in water. The initial mobile phase was composed of 50% solvent A pumped at 0.3 mL/min for 12.0 min, changed to 95% solvent A and was held constant for 4.0 min. At 16.1 min the percentage of solvent A returned to initial conditions of 50% and allowed to equilibrate for 2 min followed by an injection of the next sample. Total run time was 18 min. The retention times were 9.6 and 9.4 min for UPCDC-10205 and $^{2}H_{7}$ - UPCDC-10205, respectively (Figure 5). The minor difference in RT can be attributed to the 7 deuteriums on the internal standard which can cause slight differences interactions with the stationary phase on the column.

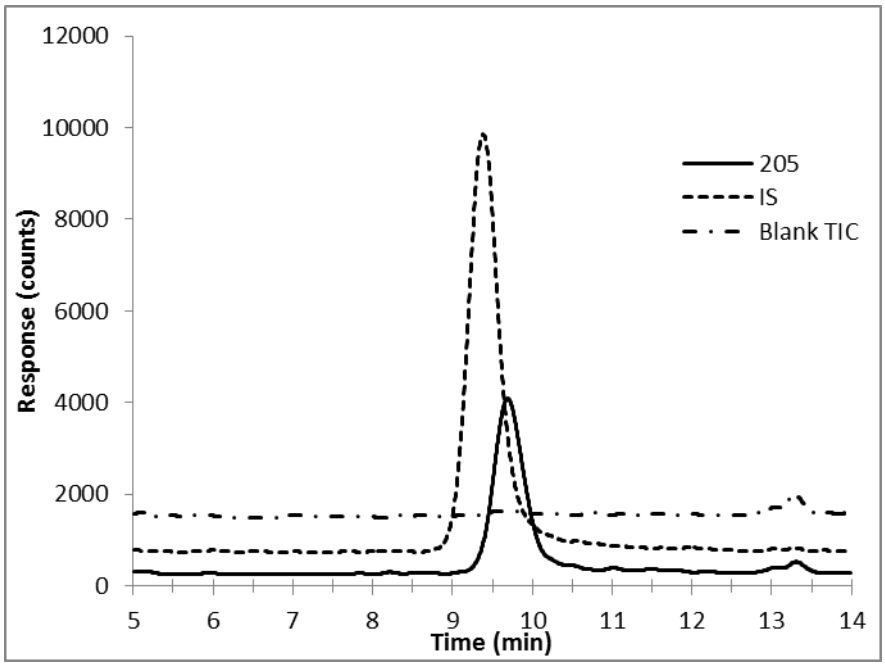

Figure 5. Chromatogram from the quantitative LC-MS assay developed for the PK study. Shown is an LLQ sample (1 ng/mL) of UPCDC-10205, the internal standard (500 count offset) and an overlaid TIC chromatogram of a blank plasma sample (offset 1000 counts).

A Waters Quattro Micro mass spectrometer (Milford, Massachusetts) was used in positive-ion MRM mode (4.5 kV capillary voltage, 30 V cone voltage, 450 °C desolvation

temp.) to monitor *m/z* 437.0>304 for UPCDC-10205 and *m/z* 444.0>304.0 for the internal standard. The postulated fragmentation pattern to obtain these transitions is seen in Figure 6.

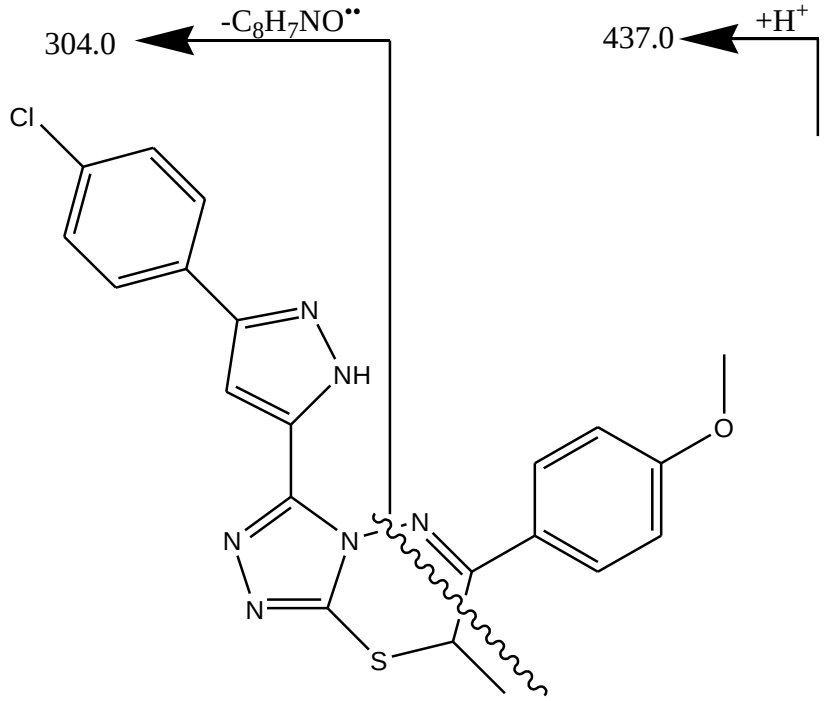

Figure 6. Postulated UPCDC-10205 fragmentation pattern. Positive ionization monitored the parent *m/z* of 437.0 and the product ion of 304.0 *m/z.*

The calibration curve had a range of 1 to 1000 ng/mL (1, 3, 10, 30, 100, 300, 500, 1000 ng/mL) and were prepared fresh in control mouse plasma obtained from Lampire Biological Labs Inc. (Ottsville, PA). Calibrators were prepared from serial dilutions of UPCDC-10205 in DMSO from a 1.0 mg/mL UPCDC-10205 stock solution that was stored at -80° C. Quality controls (QCs) were prepared in bulk using mouse plasma at three concentrations (2.5, 30, 800 ng/mL) and aliquoted to 100 µL and stored at -80 °C until days of sample analysis. Two QCs at each level were analyzed alongside each study sample batch.

Assay performance and stability was evaluated as well. The effect of 3 freeze/thaw cycles on analyte concentrations in plasma was evaluated by assaying mid QCs after they had been frozen (-80 °C) and thawed on 3 separate days and comparing the results with those of that were not frozen. The stabilities of UPCDC-10205 in plasma during sample preparation were evaluated by assaying mid QCs before and after 4 h of incubation at room temperature.

The validity of the assay in tissue homogenate was also tested by spiking untreated kidney and liver homogenate at the mid QC level and comparing it against a calibration curve prepared in mouse plasma.

2.4.3 Assay Sample Preparation

The sample volume was 100 µL of plasma or tissue homogenate. All samples were spiked with 10 µL of 0.2 µg/mL of the $^{2}H_{7}$-UPCDC-10205 internal standard. Extraction and protein precipitation were accomplished using 500 µL of acetonitrile added to each sample. Samples were vortexed using a using a Vortex Genie 2 (Scientific Industries, Bohemia, NY) and centrifuged using an Eppendorf 5415C microcentrifuge (Westbury, NY). Supernatants were transferred to borosilicate glass tubes and placed in an evaporation apparatus (Multivap Nitrogen Evaporator, Organomation Associates, Berlin, MA) set at 37 °C and evaporated under a gentle stream of nitrogen (Valley National Gases, Inc., Pittsburgh, PA). Tissues were homogenized with 3 parts PBS (*v/g*) and values were corrected for dilution after analysis.

2.4.4 Pharmacokinetic Analysis

Samples from each mouse were analyzed using the quantitative LC-MS/MS assay. The values quantitated for each of the three mice per time point were averaged to obtain a mean that

served as the representative value for that time point. PK parameters (AUC_{0-t}, $AUC_{0-\infty}$, $T_{1/2}$, V_d, and V_{ss}) were derived through non-compartmental analysis using PK Solutions (Summit PK, Montrose, CO)

2.4.5 Protein Binding

To assess the level of plasma protein binding of UPCDC-10205, a rapid equilibrium dialysis (RED) method (Thermo Scientific, Pittsburgh, PA) was used. Control mouse plasma was spiked at 1,000 ng/mL using a stock prepared in DMSO (organic < 0.1%). Four replicates of 200 µL from the spiked 1000 ng/mL plasma were placed into the RED insert placed within a Teflon plate and 350 µL of PBS (pH 7.2) was aliquoted in the opposite side of the insert. The plate was placed on a shaker in an incubator at 37 °C for 4 hours. After this time, both saline and plasma portions were isolated and stored at -80 °C until analysis. Quantitation was achieved by creating standard curve in a matrix of 1:1 PBS:plasma and prepared and analyzed using the quantitation LC-MS/MS assay (2.4.2 and 2.4.3). Samples were diluted with either PBS or plasma to match the calibrator matrix.

2.5 METABOLISM

2.5.1 Metabolite Profiling

To identify metabolites of UPCDC-10205, a series of LC-MS/MS methods were developed and utilized. Both plasma (IV 30 min 4 mg/kg) and urine (IV 0-6 hr 4 mg/kg) from

mice used in the PK study were separately evaluated and compared to their respective vehicle controls to identify unique traces in treated mouse samples. Unique traces were confirmed using a selected reaction monitoring (SRM) method that monitors specified ions. Unique trace potential metabolites were postulated by comparing the unique *m/z* trace to the parent UPCDC-10205 *m/z* (437).

2.5.2 Qualitative Metabolite Profiling LC-MS/MS assays

Sample preparation was identical to the quantification method (see 2.2.3). The LC method was extended compared to the quantitative method to a run time of 75 minutes and used a gradient to spread out eluates using a Phenomenex Luna phenyl-hexyl column (3µ, 100X2.0 mm). Mobile phase conditions for mobile phase A (acetonitrile with 0.1% formic acid) increased from the initial 5% to 55% at 0.3 mL/min for 60 min. This composition was then held at 55% for 5 minutes then increased to 80% and held for 5 additional minutes until returning to initial conditions for equilibration during the final 5 minutes.

To first identify metabolites, five sequential full mass (MS) scans were conducted using methods split into 100 *m/z* ranges to obtain a total scan range of 400-900 *m/z*. MS parameters were identical to the quantification method, with the exception of collision voltage and collision gas being turned off.

Chromatographic peaks detected in urine or plasma were analyzed for their *m/z* trace composition. These *m/z* values were then used in an SRM MS method and the samples reanalyzed. To gain structural information, product ion scans (PIS) were used to identify potential areas of metabolic alterations. Five PIS were conducted simultaneously using unique collision voltages (10, 20, 30, 40, and 50) to get a variety of fragmentation products. Fragments

obtained through the PIS were compared to parent UPCDC-10205 fragmentation to elucidate metabolite structures using ChemDraw (PerkinElmer, Waltham, MS).

The natural abundance of the stable isotope of 37-chlorine (^{37}Cl) is approximately 25%, and this was employed to fingerprint UPCDC-10205 metabolites. Unique chromatographic peaks with *m/z* traces and *m/z* +2 were considered derived from UPCDC-10205. Additionally, during the PIS, product ions were analyzed to deduce structure and by analyzing potential fragmentation patterns to achieve a postulated metabolite. The presence of an overlapping +2 *m/z* trace on a product ion can yield information on the position of metabolic alterations.

2.5.3 *In Vitro* Metabolism

Microsomes were prepared and isolated from heterozygous *Foxn1*^{nu}*/Foxn1*$^{+}$female mice as described previously (2.2.1). The microsomal pellet was stored at -80 °C until measurement of protein concentration using the Biorad assay using BSA as a standard. The incubation for glucuronide metabolism was adapted from a previously published method to allow for a 1,000 µL incubation volume.[37] The incubation mixture contained 0.1 M phosphate buffer (pH 7.4), 0.25 mg/mL microsomal protein concentration, 25 µg/mL alamethicin, 50 mM Tris-HCl, 10 mM $MgCl_2$, and a 1,000 ng/mL drug concentration. The reaction was catalyzed with the addition of 5 µM UPDGA. At 0, 15, 30, 45, and 60 minutes, 100 µL aliquots were sampled from the reaction mixture and 500 µL of acetonitrile added to terminate the reaction. 10 µL of 1.0 µg/mL internal standard ($^{2}H_7$ -UPCDC-10205) was added to each sample. Samples were processed as described previously. Samples were analyzed twice along with a standard curve produced in phosphate buffer matrix (pH 7.4) with 0.25 mg/mL BSA. The first analysis used the qualitative SRM LC-MS assay to monitor a 613 *m/z* (437+176) glucuronide channel and the second used the

quantitative MRM LC-MS assay to quantitate UPCDC-10205 substrate depletion. An incubation mixture without UPDGA cofactor was used as a negative control.

3.0 RESULTS

3.1 SELECTION OF *IN VIVO* LEAD CANDIDATE

3.1.1 LC-MS Assay

The regression was weighted $1/y^2$ and fit quadratically. Figures of a triplicate standard curve and the respective R^2 coefficient can be seen in Figure 7. A triplicate standard curve prepared prior to sample analysis revealed all four analytes were quantitated accurately (94.0-109.5%) and precisely (CV<10.1%) (Table 1). The ratio of analyte area to internal standard area was used to back calculate the concentration based off of standard curves. Quantitation using linear regression proved unsuccessful in both SRM and MRM modes. Causes of non-linearity cannot be attributable to internal standard as levels remained constant during analysis. Differences of analyte ionization at varying concentrations are most likely the cause non-linear analyte to internal standard regression. Fitting the regression quadratically fit the data best and allowed for acceptable fit.

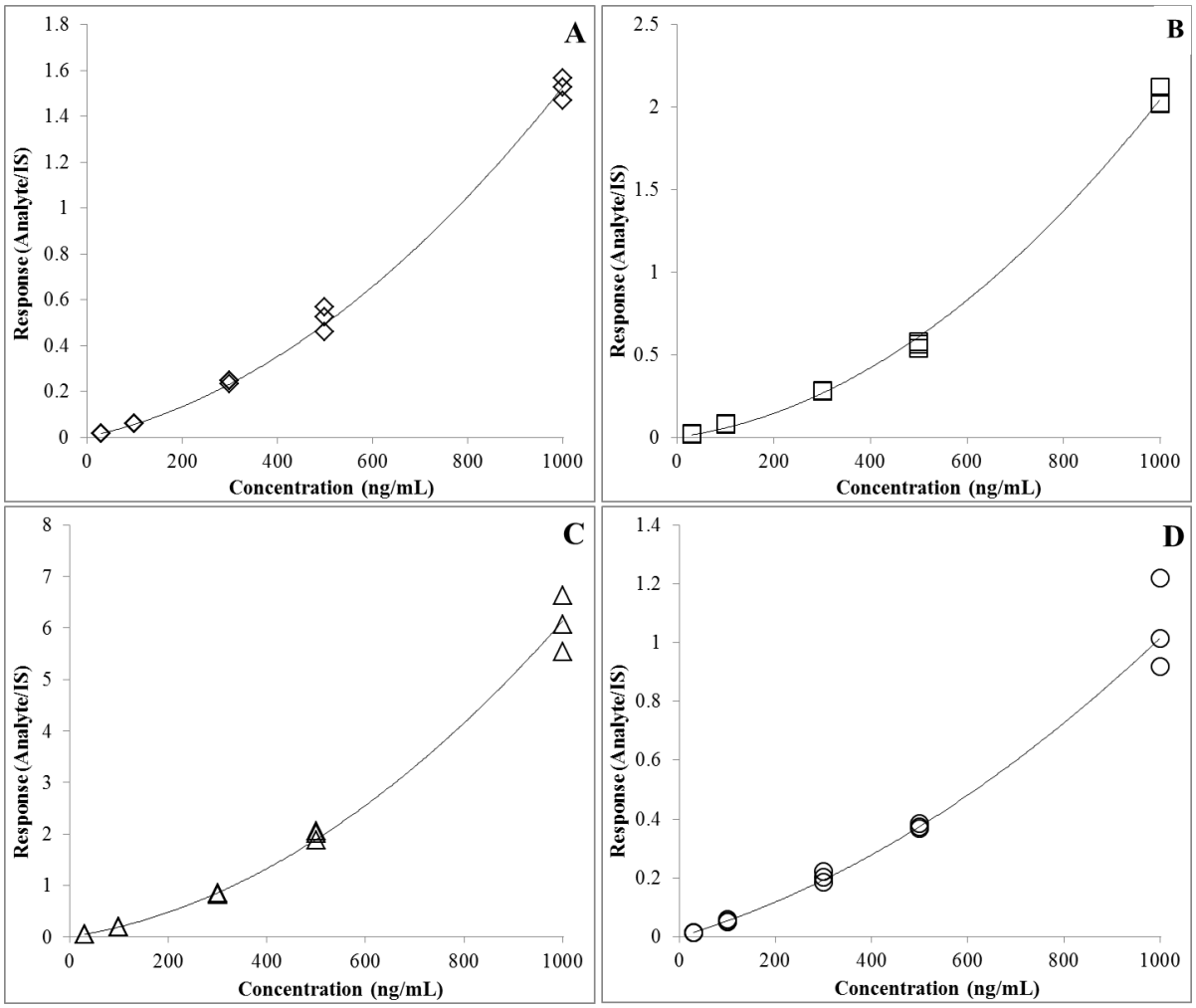

Figure 7. Triplicate standard results, quadratic regression curves ($Y=A+B*X+C*X^2$) and R2 coefficients. (A) 864669 had an R^2 of 0.994, (B) UPCDC-10205 had an R^2 of 0.988, (C) UPCDC-10305 had an R^2 of 0.995 (Δ), and (D) UPCDC-10540 had an R^2 of 0.993.

Table 1. Assay performance data of the calibration samples for STAT3 inhibitors in phosphate buffer with 0.5 mg/mL BSA

Analyte	Conc. (ng/mL)	Bias (%)	Precision (%)
UPCDC-10205	30	1.0	9.4
	100	-9.5	3.7
	300	2.9	0.9
	500	6.0	2.5
	1000	-6.4	1.6
UPCDC-10305	30	-1.0	7.8
	100	0.0	1.1
	300	1.3	1.1
	500	-2.7	2.8
	1000	0.6	5.1
864669	30	-1.4	4.8
	100	4.0	0.1
	300	1.0	2.4
	500	-3.3	7.3
	1000	-3.9	2.0
UPCDC-10540	30	-1.3	4.0
	100	3.2	10.1
	300	-3.8	5.5
	500	-3.5	7.8
	1000	0.4	9.5

N=3; from a single triplicate results

3.1.2 Substrate Depletion

All sample concentrations fell within the standard calibration curve range. Concentration values were expressed as a % of the average starting concentration (0 min), seen in Figure 8.

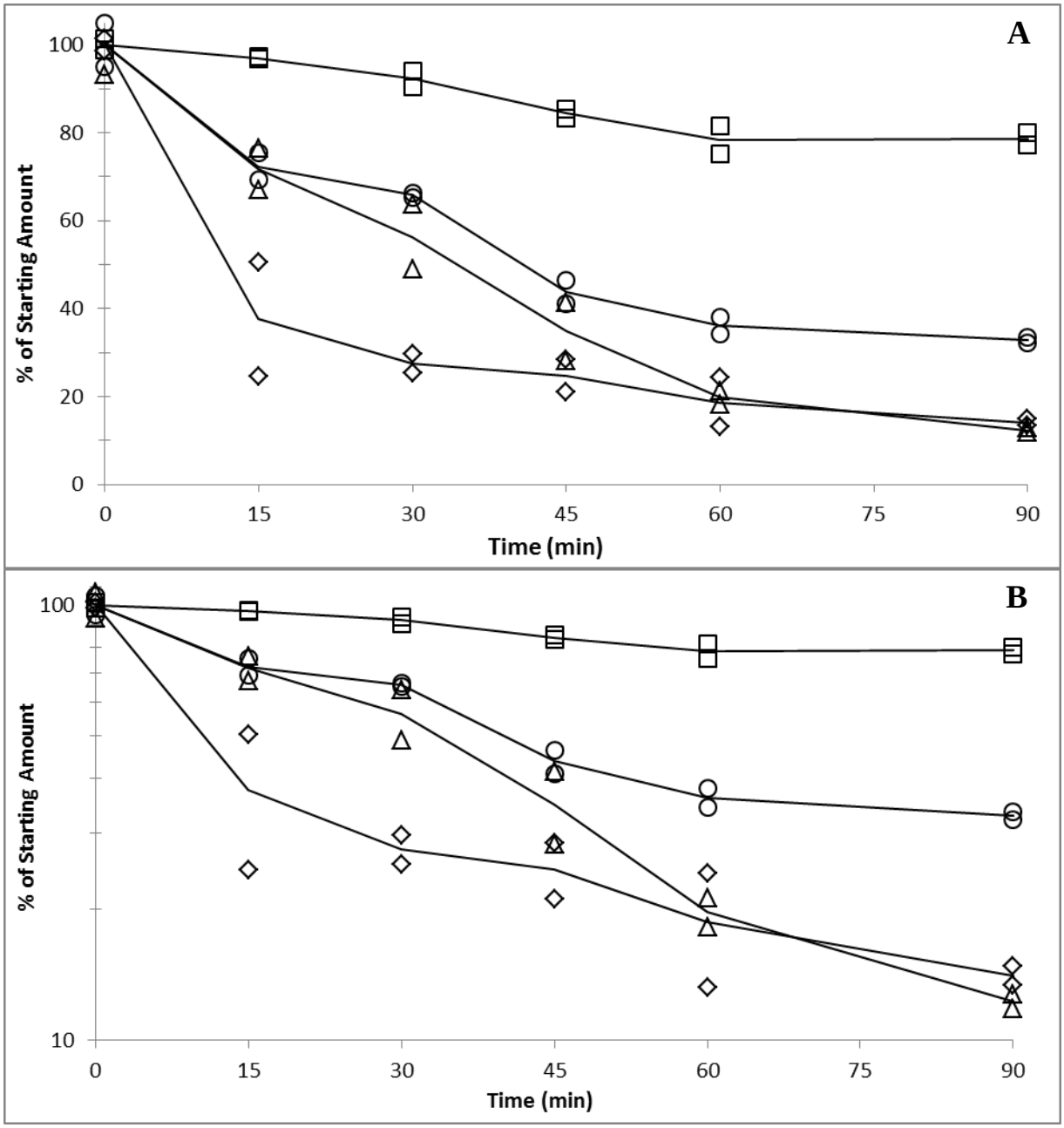

Figure 8. Microsomal incubation of 864669 (◊), UPCDC-10205 (□), UPCDC-10305 (Δ), and UPCDC-10540 (○) in A) linear and B) logarithmic y-axes.

UPCDC-10205 had the largest proportion of the starting amount remaining after the 90 minute incubation with 78.6% remained after 90 minutes compared to 14.1% for 864669, 12.3%

for UPCDC-10305 and 32.9% for UPCDC-10540. UPCDC-10205 was prioritized for *in vivo experimentation* based on this metabolic stability.

3.2 TOXICITY STUDIES

3.2.1 Single Dose Toxicity Study

After administration of the maximum soluble dose of UPCDC-10205 at 4 mg/kg in 10% Solutol™ HS (0.4 mg/mL at a volume of 0.01 ml/g body weight), mice appeared normal and similar to vehicle dosed control mice. Clinical observations of the male and female mice indicated mice were healthy for the following 14 day observation period. All mice gained weight during the observation period with no apparent weight loss measured within the first 24 h after injection (Figure 9). Upon necropsy, no gross pathology was detected in any of the mice. One male had bite marks and local irritation on the skin between the scapulae where he had been bitten. The testes in this mouse were also smaller by about 30% compared to his cage mates and his spleen weight was slightly elevated, most likely due to infection. All other male mice appeared normal. The administrable maximum soluble dose at 4 mg/kg was determined to be the maximum tolerable dose (MTD).

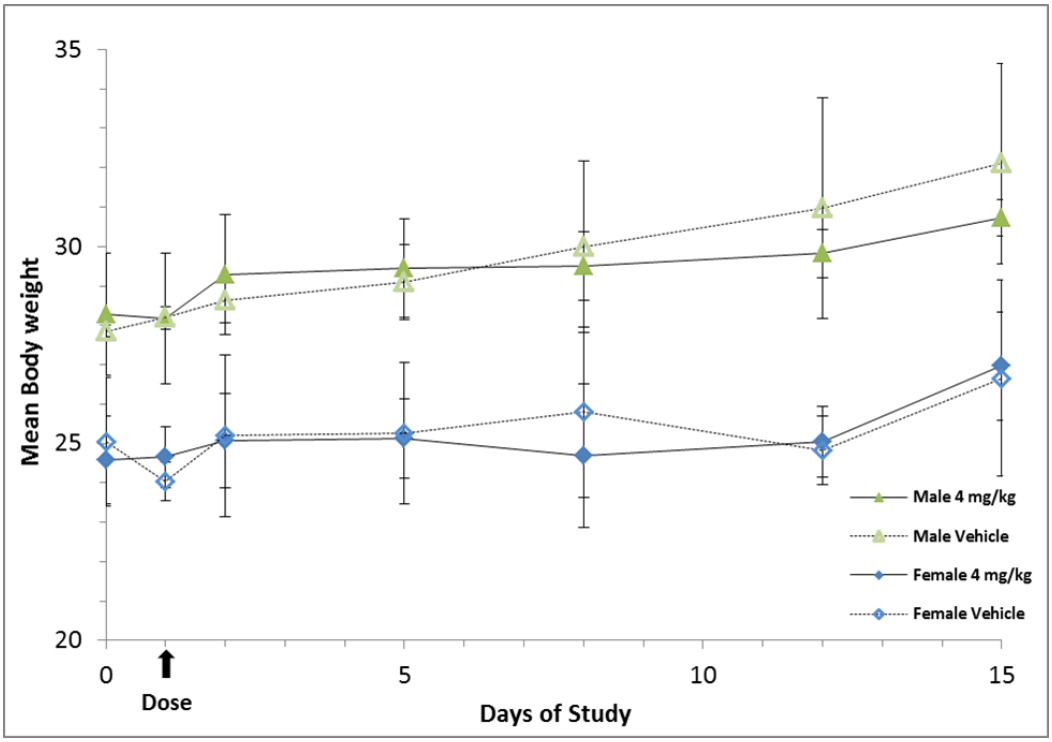

Figure 9. Single dose toxicity study results of average mouse body weights (N=3) before and following a single IV injection of UPCDC-10205 at 4 mg/kg. Error bars represent ±1 SD.

3.2.2 Multiple Dose Toxicity Study

Because there were no obvious differences between sexes in both clinical observations and body weights between vehicle treated and UPCDC-10205 treated mice, only female Foxn nu/+ mice (N=20) were used for the multiple dose toxicity study. Groups of mice were dosed IV daily for five days (QDx5) with vehicle, 4 mg/kg, 2.7 mg/kg (2/3 single dose MTD), and 1.3 mg/kg (1/3 single dose MTD). No signs or symptoms of toxicity were detected during the five day treatment period or the 14 day observation period. All mice gained weight during the study and weights between treatment groups showed no statistical differences to the vehicle control group (Figure 10). The mice remained healthy and there we no signs of gross pathology upon necropsy.

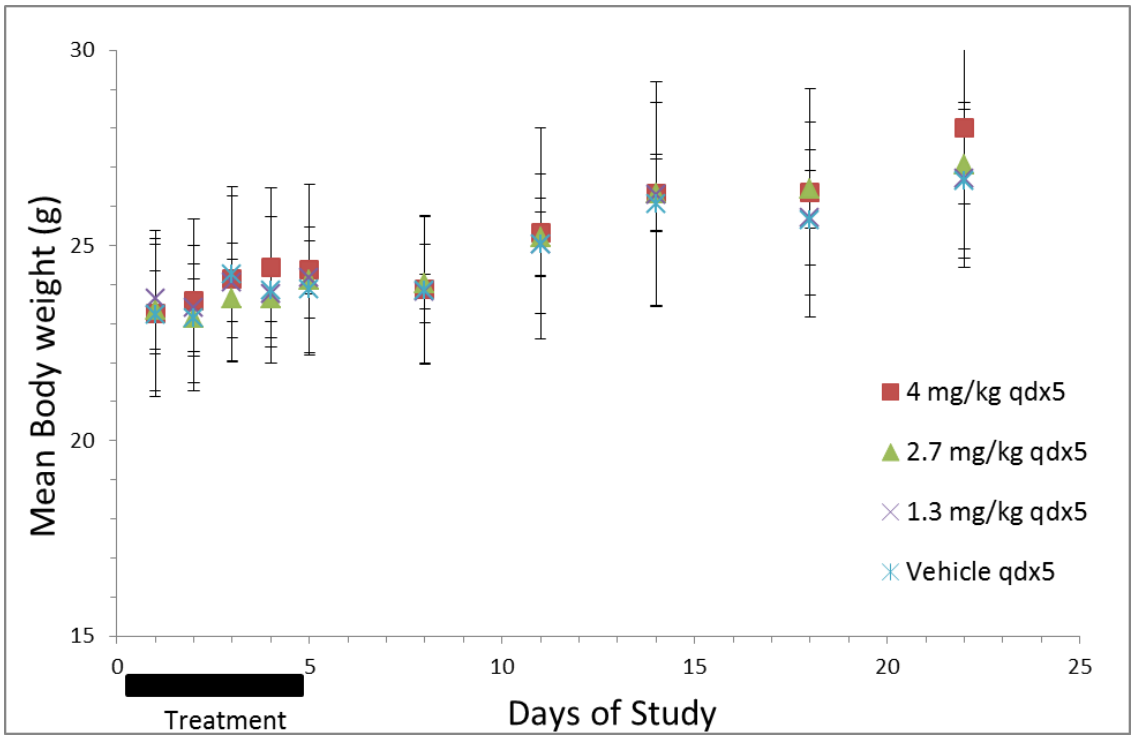

Figure 10. Multiple dose toxicity study. Averaged mouse body weights during and after QDx5 IV administration of UPCDC-10205 at IV daily for QDx5 with vehicle, 4 mg/kg, 2.7 mg/kg, and 1.3 mg/kg given to female mice. Error bars represent ±1 SD.

3.3 PHARMACOKINETICS

3.3.1 Quantitative LC-MS/MS Assay

The regression was weighted $1/y^2$ and fit linearly (Y=A+B*X, Y=0.124+0.074*X) with and R^2 coefficient of 0.998 (Figure 11). A triplicate standard curve prepared prior to sample analysis revealed UPCDC-10205 was quantitated accurately (93.7-108.1%) and precisely (CV< 8.3%), see Table 2. The ratio of analyte area to internal standard area was used to back calculate the concentration based off of a standard curve.

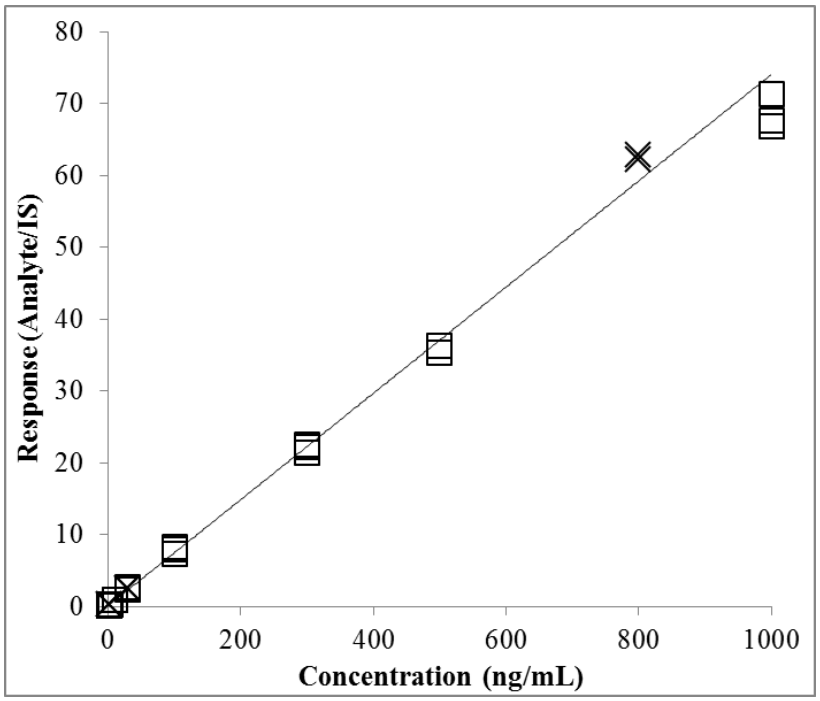

Figure 11. Triplicate standard curve results from the quantitative LC-MS/MS assay for UPCDC-10205 showing calibrators (□), QCs (✕) and linear $1/y^2$ weighted regression curve (Y=0.124+0.074*X).

Table 2. Assay performance data of the calibration samples of UPCDC-10205 in mouse plasma.

Conc. (ng/mL)	Bias (%)	Precision (%)
1	-5.4	8.0
3	6.3	8.3
10	-3.0	0.8
30	5.0	3.7
100	-8.1	3.7
300	-2.9	4.2
500	0.4	3.4
1000	1.8	3.7

N=3; from a triplicate calibration curve prepared in mouse plasma.

The recovery of UPCDC-10205 at the QCM was 46.2%, with a CV of 8.0%. Ion-suppression at the QCM was 8.2 with a CV of 6.6% (Table 3). The stability in plasma after 3 freeze thaw cycles (-80 °C to RT) at the QCM level was 111.5%. The stability in plasma after 4 hours at RT at the QCM level was 100.8% (Table 4). Recovery of the analytes in kidney and liver tissue homogenates analyzed against a plasma calibration curve ranged from 98.8– 105.1% with CVs ranging from 2.3 –7.4% (

Table **5**).

Table 3. Recovery of UPCDC-10205 from mouse plasma and respective ion suppressions in mouse plasma extract, with coefficients of variation (CV).

Concentration (ng/mL)		Recovery (%)	CV (%)	Ion suppression (%)	CV (%)
QCM	30	46.2	8.0	8.19	6.6

N=4

Table 4. Stability of UPCDC-10205 under varying conditions.

Storage condition	Concentration (ng/mL)		Stability (%)	CV (%)
F-T Cycle (3x)	QCM	30	101.3	11.6
Bench (RT) 4 h	QCM	30	100.8	9.6

N=4

Table 5. Recovery of UPCDC-10205 from mouse liver and kidney homogenates.

Tissue	Concentration (ng/mL)		Recovery (%)	CV (%)
Liver	QCL	2.5	99.9	5.5
	QCM	30	102.7	4.0
	QCH	800	105.1	4.0
Kidney	QCL	2.5	102.1	7.4
	QCM	30	98.8	4.9
	QCH	800	100.4	2.3

N=4

3.3.2 Pharmacokinetics

All PK parameters were analyzed using mean concentrations (N=3) of the three designated mice per time point. AUC_{0-t} comparisons between administration forms are provided in Table 6 and C_{max} and T_{max} comparisons in Table 7. UPCDC-10205 levels in pooled urine from the IV 4 mg/kg mice represented 0.0011% (5.4 ng/mL) of the total amount administered for 0-6 h collection and 0.0010% (1.6 ng/mL) for 6-24 h collection. Levels in pooled urine from the PO

4 mg/kg mice represented 0.0077% (42 ng/mL) of the total dose between 0-6 h. Quantitation of UPCDC-10205 in the 6-24 h as well as all urine samples from the PO 30 mg/kg in 1% CMC had concentrations below the LLQ.

Table 6. UPCDC-10205 AUC_{0-t} (ng·mL-1·h) in tissues as a measure of exposure

Route	mg/kg	Plasma	F	Liver	Kidney	Lung	RBC	Muscle	Brain
IV	4	1021	100	1472	3240	2681	556	1634	1731
PO	4	52.1	5.1	300	428	630	23.5	91.4	30.0
CMC	30	25.7	0.3	542	272	186	-	140	33.4

UPCDC-10205 AUC_{0-t} calculated non-compartmentally. F represents the fraction of IV plasma AUC_{0-t} to PO plasma AUC_{0-t} normalized to dose and multiplied by 100.

Table 7. Cmax and Tmax of UPCDC-10205 in administered mice.

	mg/kg		Plasma	Liver	Kidney	Lung	RBC	Muscle	Brain
IV	4	C_{max}	1708	2779	4621	4494	980	1900	1643
		Observed T_{max}	0.08	0.08	0.08	0.08	0.08	0.25	0.25
PO	4	C_{max}	35.0	220	308	414	16.0	51.2	15.4
		Observed T_{max}	0.5	0.08	0.5	0.08	0.5	1.0	1.0
CMC	30	C_{max}	6.7	564	404	331	-	189	49.0
		Observed T_{max}	1.0	0.08	0.08	0.08	-	0.08	0.08

C_{max} and T_{max} were derived from averages (N=3).

IV 4 mg/kg Pharmacokinetics

The observed plasma C_{max} for IV administered UPCDC-10205 was 1,707 ng/mL (± 455 ng/mL) and occurred 5 minutes after injection. Plasma UPCDC-10205 levels were below the lower limit of quantitation (LLQ) by the 6 h time point. The *in vivo* profile appears biphasic indicating two compartments. PK parameters are listed in Table 8 and plasma, liver, lung, kidney, brain, skeletal muscle and red blood cell values can be viewed in Figure 12. The half-life in plasma was calculated non-compartmentally to be 0.6 hours and the AUC_{0-t} to be 1021 ng•h/ml.

Table 8. PK of IV UPCDC-10205 4 mg/kg dosed mice.

		C_{max} ng/mL	Observed T_{max} h	$T_{1/2}$ h	AUC $_{0-t}$ ng/mL*hr	AUC $_{0-\infty}$ ng/mL*hr	Cl mL/hr/kg	V_d mL/kg	V_{ss} mL/kg
Plasma		1708	0.08	0.6	1022	1022	3913	3378	2038
								% AUC Tissue/Plasma	
Compartment	Liver	2779	0.08	1.3	1472	1484	2695	145	
	Kidney	4621	0.08	0.7	3240	3245	1232	318	
	Lung	4494	0.08	0.6	2682	2683	1491	262	
	RBC	980	0.08	0.7	556.3	560	7141	55	
	Muscle	1900	0.25	0.5	1634	1635	2447	160	
	Brain	1643	0.25	1.1	1731	1746	2291	171	

Results were analyzed non-compartmentally using composite concentration values of mice plasma or tissues (N=3). $T_{1/2}$, AUC_{0-t}, AUC $_{0-\infty}$, Cl, V_d and V_{ss} were obtained through non-compartmental analysis.

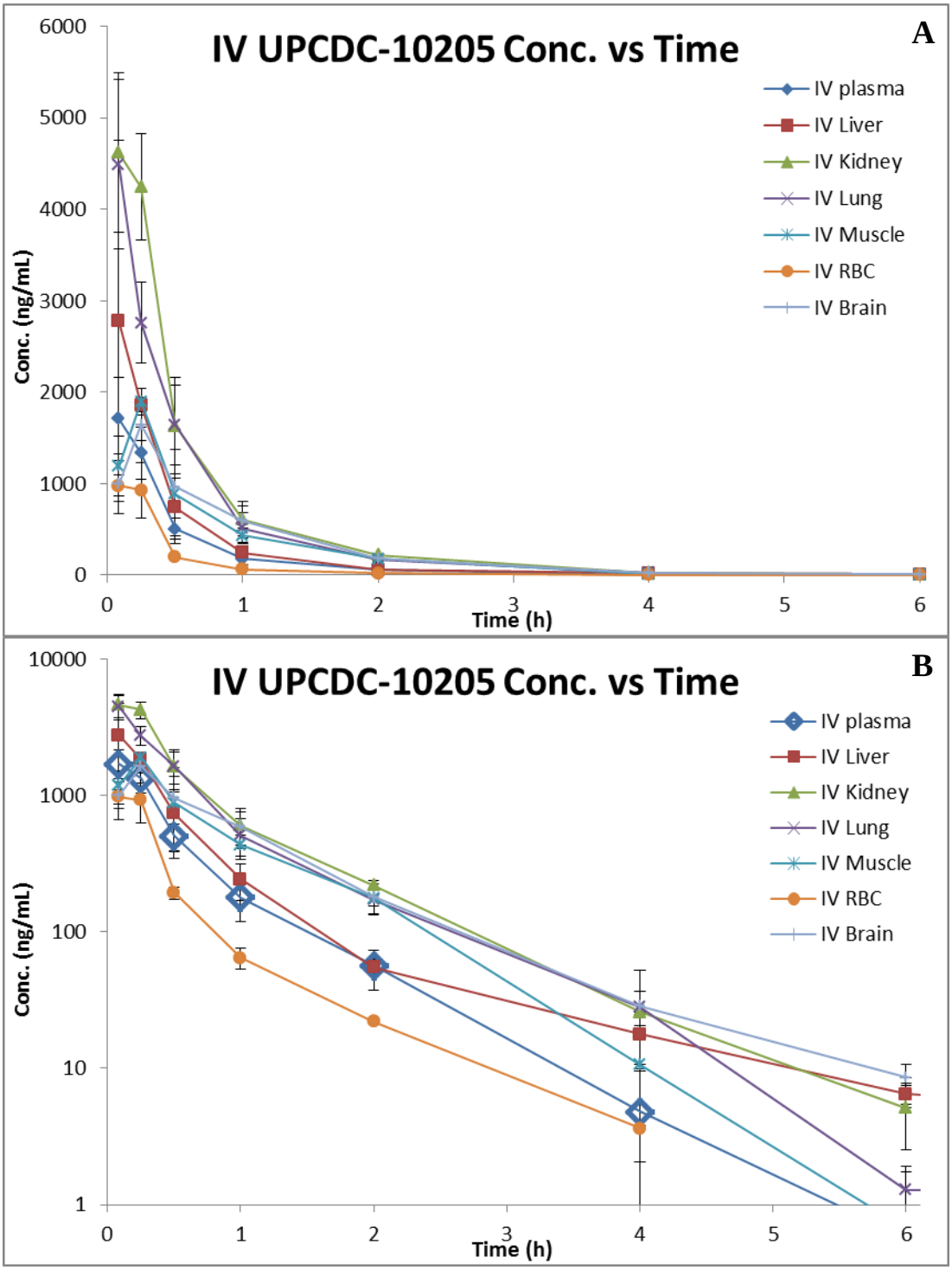

Figure 12. Concentration vs time results following IV administration at 4 mg/kg UPCDC-10205. Points represent the mean of the mice (N=3) and error bars represent ±1 SD. A) linear and B) logarithmic y axis.

PO 4 mg/kg Pharmacokinetics

The C_{max} for orally administered UPCDC-10205 at 4 mg/kg was 35.0 ng/mL and occurred at 0.5 hours after administration. Plasma UPCDC-10205 concentrations were below the LLQ after the 2 h time point. The *in vivo* profile appears triphasic indicating two compartments with an absorption phase. PK parameters are listed in Table 9 and the plasma, liver, lung, kidney, brain, skeletal muscle and red blood cell values can be viewed in Figure 13. The half-life was calculated non-compartmentally to be 0.60 h and the $AUC_{0\text{-}t}$ to be 52.1 ng•h/ml. To calculate the percent bioavailability, the following equation was used:

$$F = \frac{AUC_{Oral}}{AUC_{IV}} \times \frac{Dose_{IV}}{Dose_{Oral}} \times 100$$

Equation 1. Equation for percent bioavailability.

The resulting oral percent bioavailability for UPCDC-10205 was determined to be 5.2%.

Table 9. PK of PO UPCDC-10205 4 mg/kg dosed mice.

		C_{max} ng/mL	Observed T_{max} h	$T_{1/2}$ h	AUC $_{0\text{-}t}$ ng/mL*hr	AUC $_{0\text{-}\infty}$ ng/mL*hr	Cl mL/hr/kg	V_d mL/kg	V_{ss} mL/kg
Plasma		35.0	0.5	0.8	52	53.4	74858	88511	79810
								% AUC Tissue/Plasma	
Compartment	Liver	220	0.08	0.9	300	301	13287	563	
	Kidney	308	0.50	1.2	428	435	9191	815	
	Lung	414	0.08	0.4	629	630	6345	1180	
	RBC	16	0.50	0.3	24	24	168859	44	
	Muscle	51	1.00	0.5	91	92	43503	172	
	Brain	15	1.00	0.4	29	31	131140	57	

Results were analyzed non-compartmentally using composite concentration values of mice plasma or tissues (N=3). $T_{1/2}$, $AUC_{0\text{-}t}$, AUC $_{0\text{-}\infty}$, Cl, V_d and V_{ss} were obtained through non-compartmental analysis.

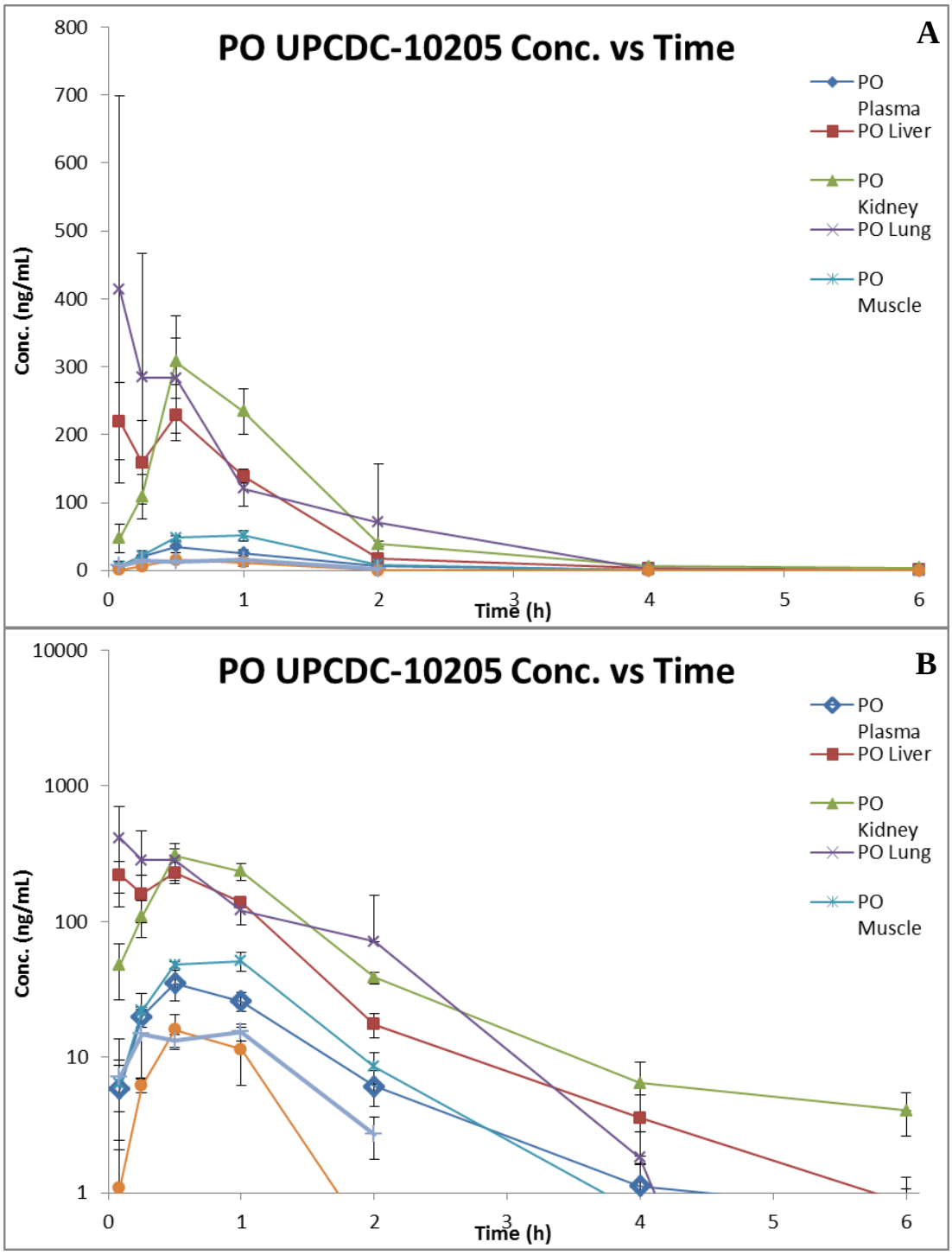

Figure 13. Concentration vs time results following PO administration at 4 mg/kg UPCDC-10205 in 10% Solutol™ HS15. Points represent the mean of the mice (N=3) and error bars represent ±1 SD. A) linear and B) logarithmic y axis.

Carboxymethyl Cellulose PO 30 mg/kg Pharmacokinetics

The C_{max} for PO administered UPCDC-10205 at 30 mg/kg CMC suspension was 6.7 ng/mL and occurred at 1.0 h after administration. The half-life was 3.4 h and calculated non-compartmentally to be 3.4 h and the AUC_{0-t} to be 25.7 ng·ml-1·hr. Dissolution from the suspension appeared to be the rate limiting step for absorption. PK parameters are listed in Table 10 and plasma, liver, lung, kidney, brain, and skeletal muscle values can be viewed in Figure 14. Using Equation 1, the percent bioavailability was 0.3%.

Table 10. PK of PO UPCDC-10205 30 mg/kg in 1% CMC dosed mice.

		C_{max} ng/mL	Observed T_{max} h	$T_{1/2}$ h	AUC $_{0-t}$ ng/mL*hr	AUC $_{0-\infty}$ ng/mL*hr	Cl mL/hr/kg	V_d mL/kg	V_{ss} mL/kg
Plasma		6.7	1.00	3.4	26	38	104699	507504	552212
								% AUC Tissue/Plasma	
Compartment	Liver	564	0.08	1.2	542	557	10462	1458	
	Kidney	404	0.08	4.2	272	385	10403	1006	
	Lung	331	0.08	3.6	185	238	16819	623	
	Muscle	189	0.08	1.7	140	149	26897	389	
	Brain	49	0.08	0.9	33	35	113948	92	

Results were analyzed non-compartmentally using composite concentration values of mice plasma or tissues (N=3).

$T_{1/2}$, AUC_{0-t}, AUC $_{0-\infty}$, Cl, V_d and V_{ss} were obtained through non-compartmental analysis.

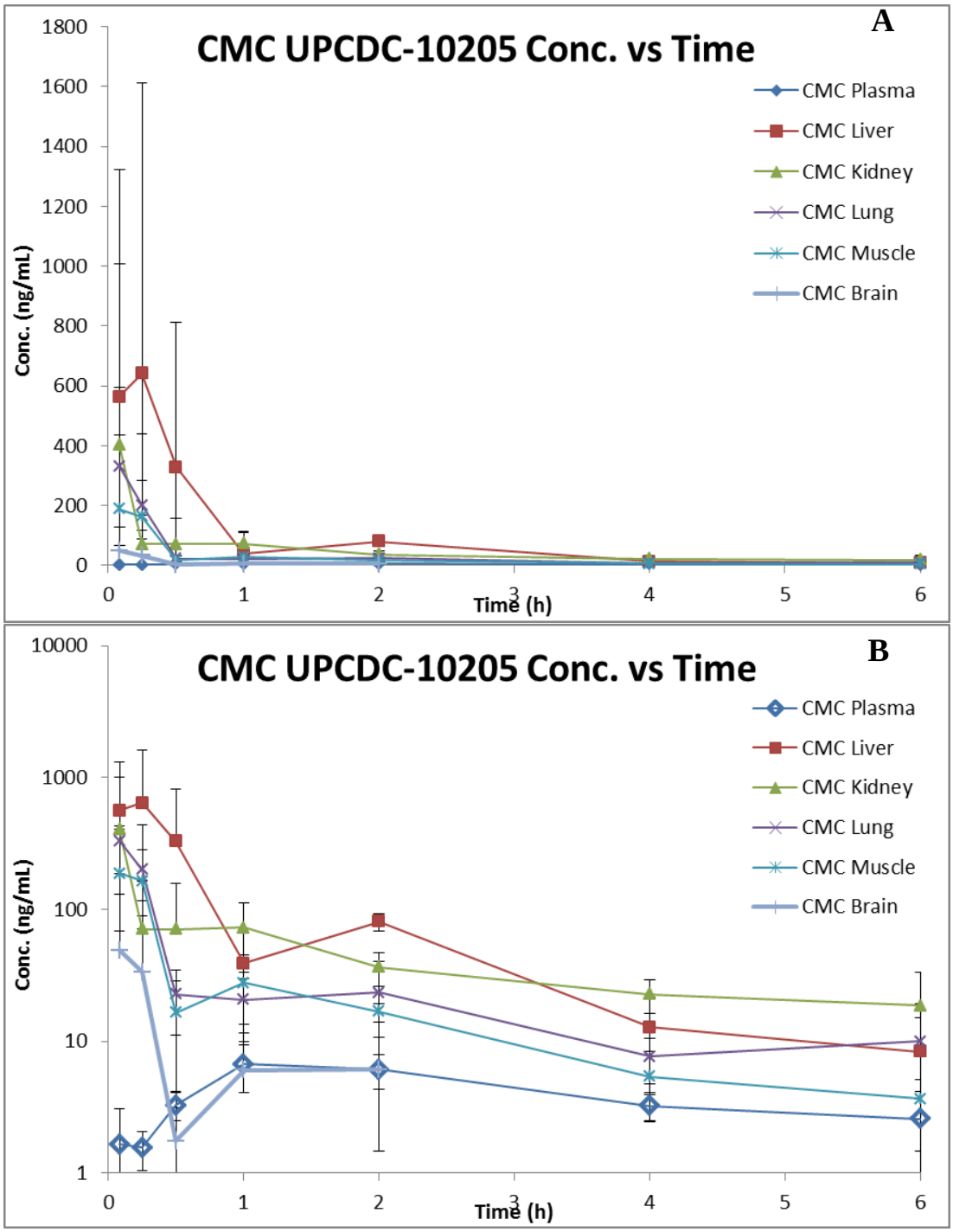

Figure 14. Concentration vs time results following PO administration at 30 mg/kg UPCDC-10205 in 1% CMC. Points represent the mean of the mice (N=3) and error bars represent ±1 SD. A) linear and B) logarithmic y axis.

3.3.2.1 Protein Binding

The average from the 4 replicates in the plasma portion of the RED device was 1,282 ng/mL and the value detected in the saline buffer portion was below the 1 ng/mL LLQ of the LC-MS/MS assay. Although below the LLQ, using the back calculated concentration of the PBS concentration yielded an average value of 0.2 ng/mL (Table 11). The ratio of saline to plasma components multiplied by 100 yielded plasma protein binding amount of 99.98%. Defining the PBS samples as the LLQ (1 ng/mL) shows that plasma protein binding is >99.92%

Table 11. RED analysis of UPCDC-10205 plasma protein binding

Plasma		PBS	
1	1260.0	1	0.24
2	1242.2	2	0.23
3	1288.9	3	0.23
4	1336.2	4	0.24
Mean	1281.8	Mean	0.23
(1-([PBS]/[Plasma]))*100=			**99.98**

LC-MS/MS analysis of RED protein binding experiment of UPCDC-10205 (n=4) after a four hour incubation at 37°C.

3.4 METABOLISM

3.4.1 Results

3.4.1.1 *In vivo* Metabolite Profiling

Unbiased MS scans of urine (0-6 hour pooled) and plasma (30 min 4 mg/kg IV) produced multiple peaks within a range of 400 to 900 *m/z,* as seen in Figure 15A and Figure 16A, respectively. A single unique peak at a retention time of 43.6 min was found in treated mouse urine and plasma compared to vehicle control samples in both the 400-500 and 600-700 MS scans (Figure 15B and Figure 16B). MS scans from the 600-700 *m/z* range showed the underlying spectra composition of the 43.6 min peak in urine and plasma identified the *m/z* traces of 613 and 615 (Figure 17). 612 is the postulated molecular weight of a direct glucuronide conjugate of UPCDC-10205 (436 + 176 = 612). The presence of a smaller (1/3rd) +2 *m/z* trace of 615 at the same RT confirm the presence of chlorine to fingerprint the glucuronide conjugate due to the natural isotopic abundance of ^{37}Cl.

Traces of 437 and 439 were also seen in urine and plasma at the same RT from the 400-500 MS scan (Figure 18). 437 and 439 *m/z* traces at the 43.6 min peak are most likely due to in-source fragmentation, where the glucuronide is cleaved from UPCDC-10205 conjugated glucuronide after chromatographic separation. Assay setup showed UPCDC-10205 to have an RT of 52.0 min and this was observed at this RT in the 400-500 MS scan in plasma but not urine (Figure 19).

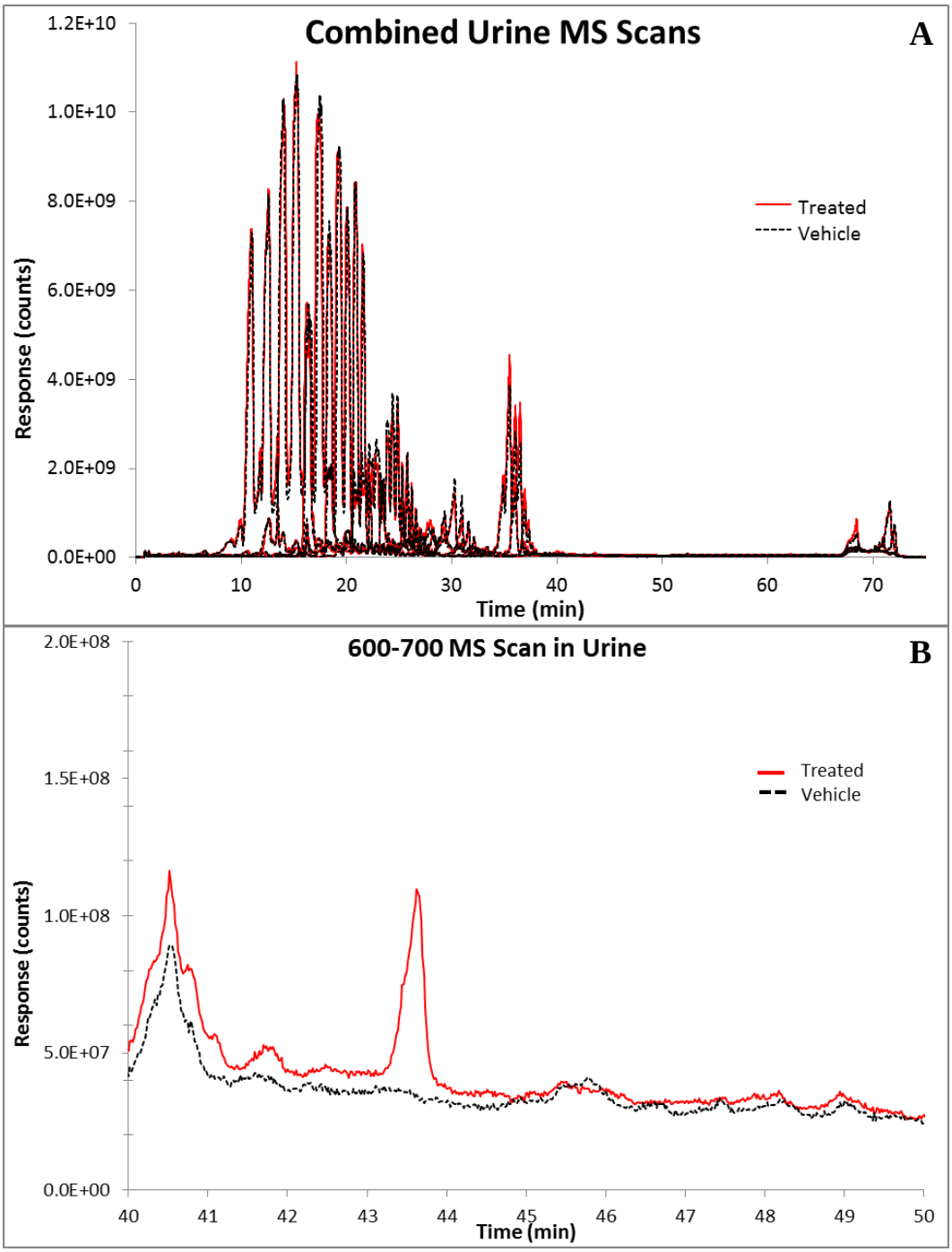

Figure 15. Urine metabolite scan using five combined MS scans (400-900 m/z) for IV treated 4 mg/kg UPCDC-10205 and vehicle control mouse urine (pooled 0-6 hr) showing A) combined scans and B) the 40-50 min region of the 600-700 MS scan and a unique peak within treated mouse urine indicating a metabolite.

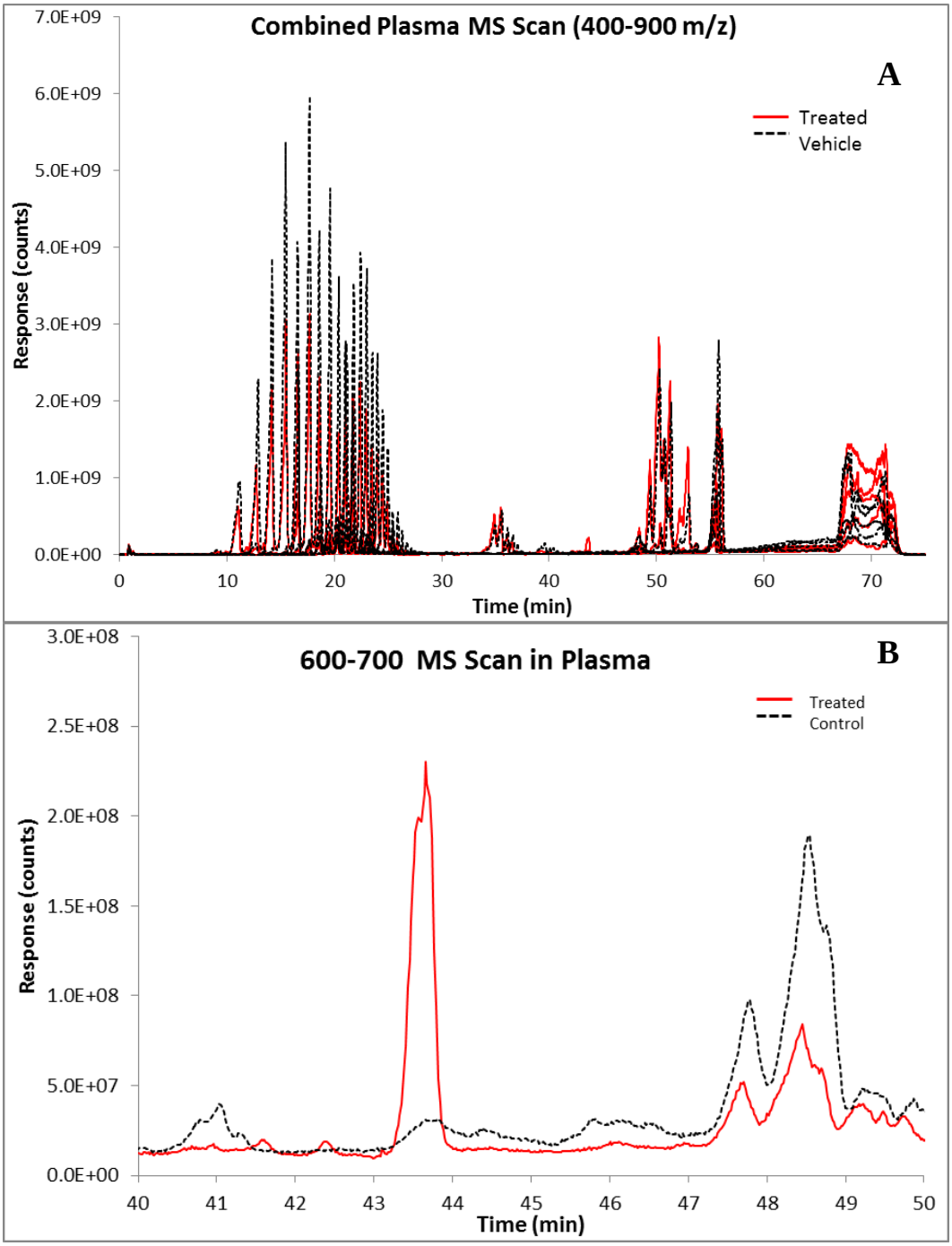

Figure 16. Plasma metabolite scan using five combined MS scans (400-900 m/z) for IV treated 4 mg/kg UPCDC-10205 and vehicle control mouse plasma (30 min) to show A) combined scans and B) the 40-50 min region of the 600-700 MS scan and a unique peak within treated mouse plasma indicating a metabolite.

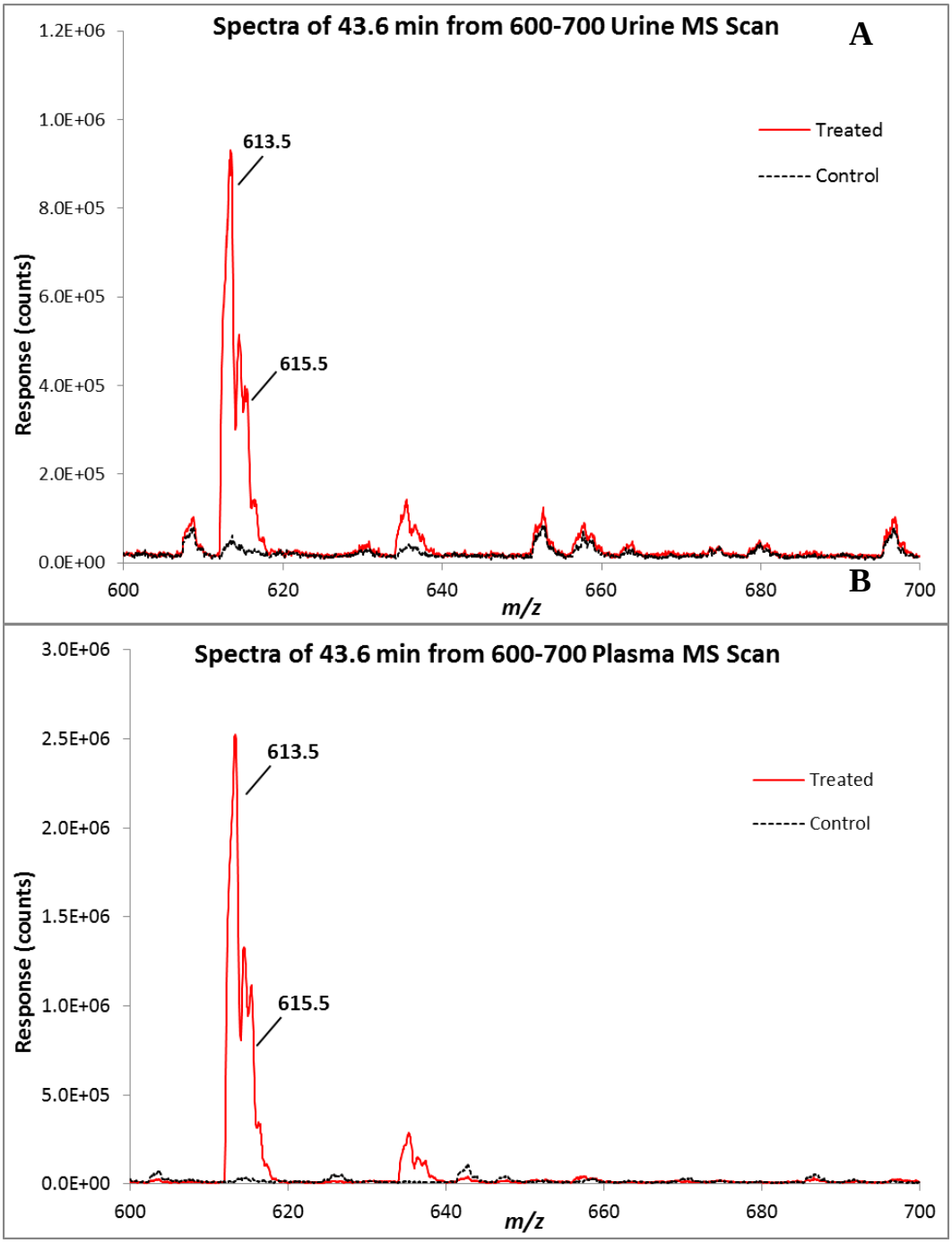

Figure 17. Spectra of the unique the 43.6 min peak from the 600-700 MS Scan of IV treated 4 mg/kg in A) urine (pooled 0-6h) and B) plasma (30 min) along with their respective controls.

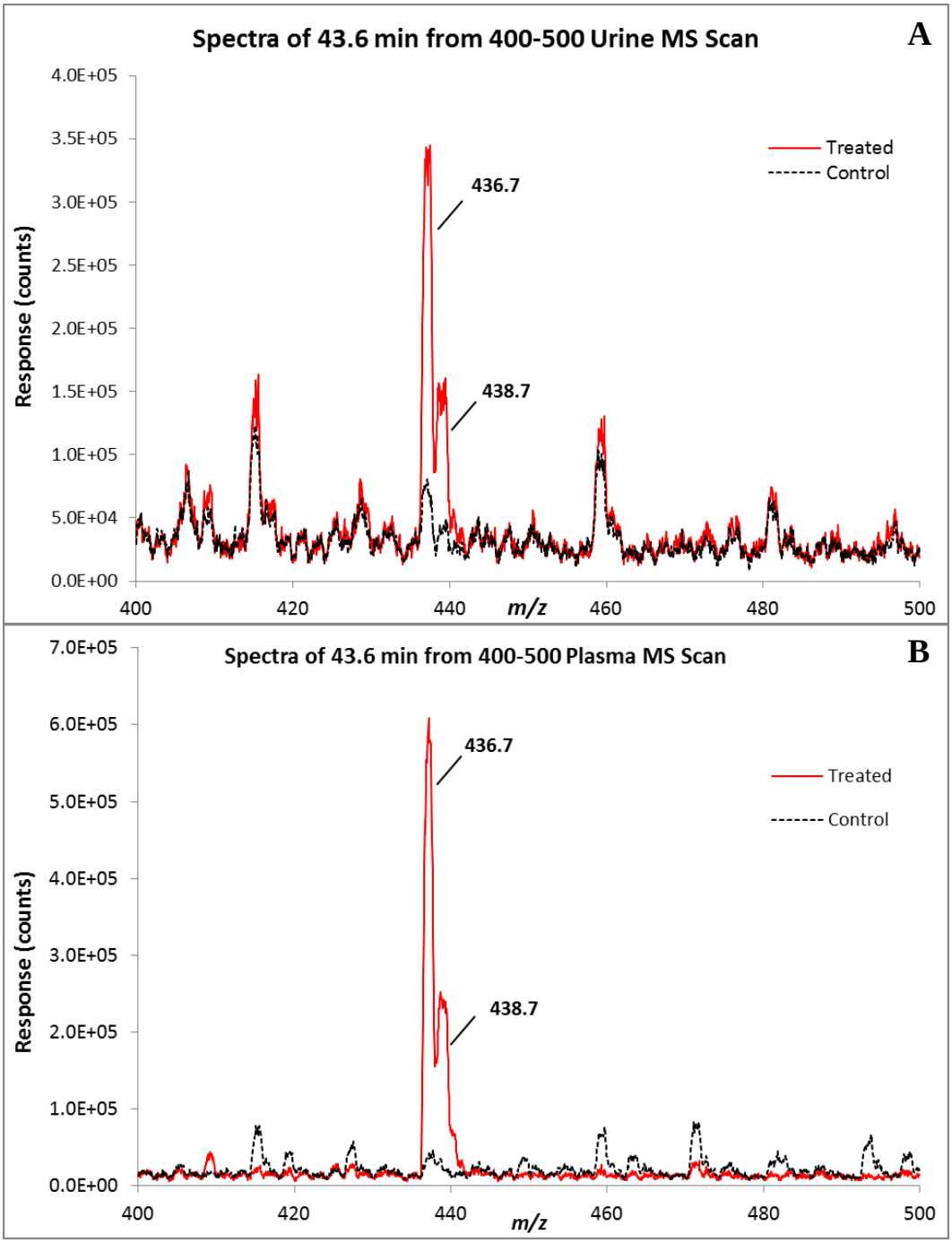

Figure 18. Spectra of the unique the 43.6 min peak from the 400-500 MS Scan of IV treated 4 mg/kg in A) urine (pooled 0-6h) and B) plasma (30 min) along with their respective controls.

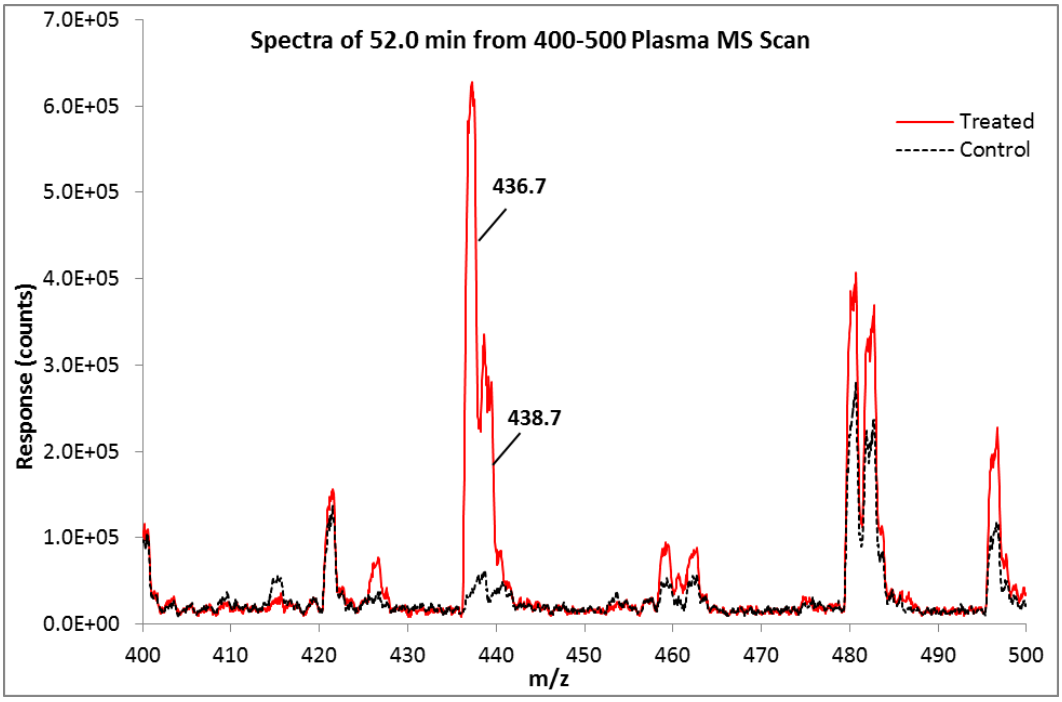

Figure 19. Spectra of the unique the 52.0 min peak from the 400-500 MS Scan of IV treated 4 mg/kg in plasma (30 min) and control plasma.

The SRM method conducted on plasma to confirm the presence of the glucuronide conjugate monitored 613 437 *m/z* yielded the similar results to the MS scan (Figure 20).

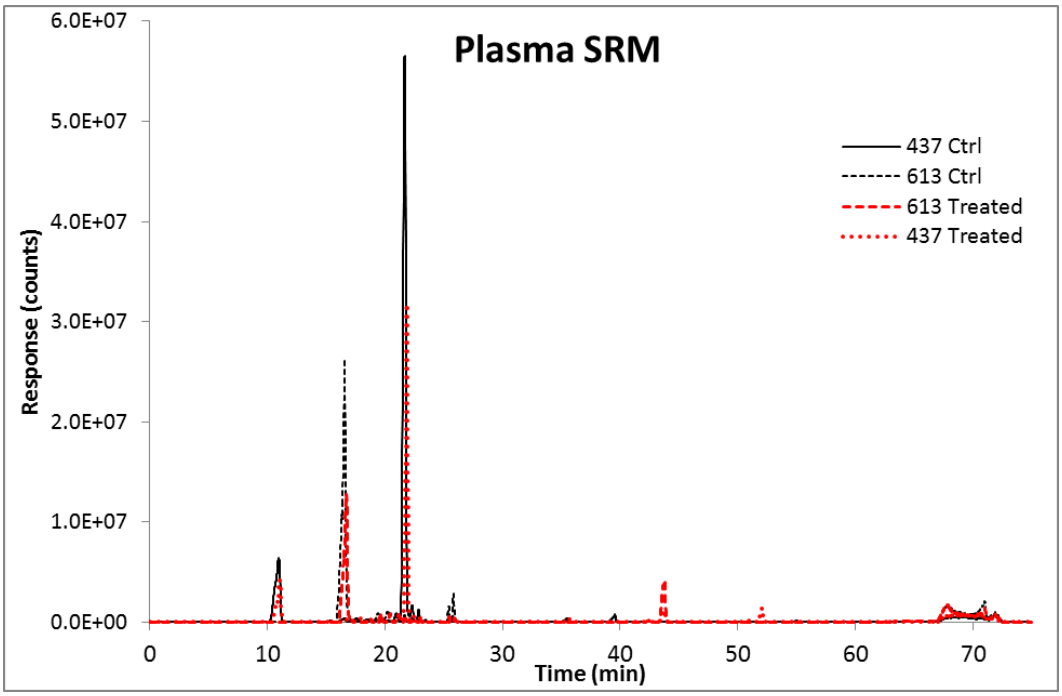

Figure 20. Combined SRM chromatograms of the 613 and 437 m/z channels in treated IV 4 mg/kg UPCDC-10205 and vehicle control plasma.

The product ion scan (PIS) of the 613 *m/z* channel (using a collision voltage of 20V) in plasma samples revealed unique product ions of 477 and 479 *m/z* at the 43.2 min RT peak (Figure 21). This spectra pattern reveals a similar ^{37}Cl fingerprint seen in UPCDC-10205 spectra. The *m/z* is greater than the parent (437), indicating the glucuronide is most likely conjugated but a portion of the parent has been fragmented. Not enough information was available to use the 477 *m/z* product ion to deduce any structural changes. Based on available electron pairs on the parent structure, it is postulated that the glucuronide is directly conjugated to either nitrogen of the pyrazole group of UPCDC-10205 (Figure 22).

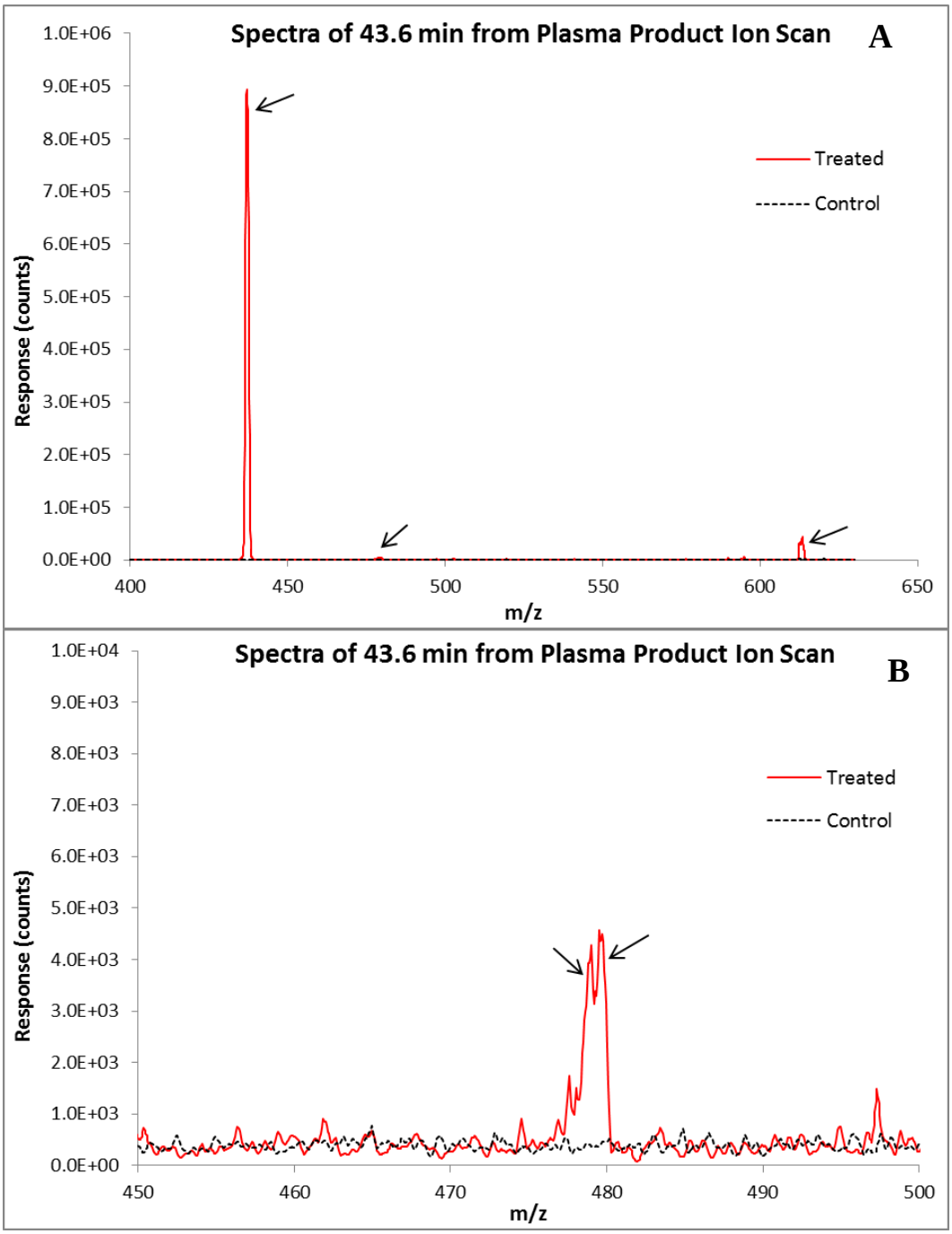

Figure 21. A)Spectra of the 613 *m/z* product ion scan from the 43.6 min peak in both treated and vehicle control mouse plasma. Arrows show product ions of 437 (UPCDC-10205), 477 (unique) and 613 (unfragmented parent mass). B) Magnified spectra showing product ions of 477(^{35}Cl) and 479 (^{37}Cl).

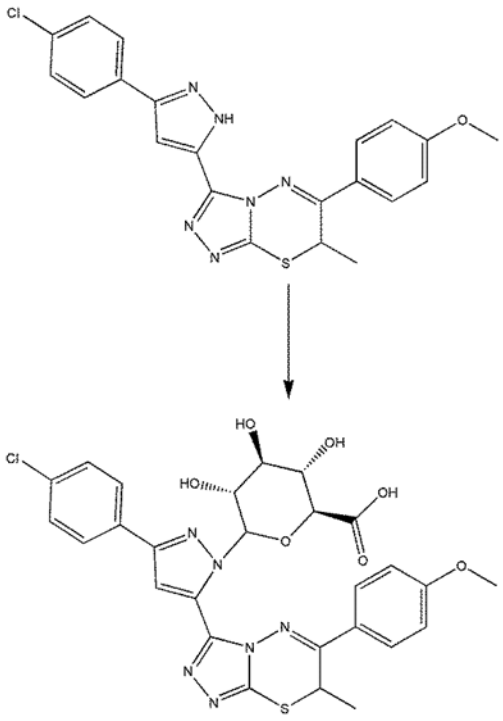

Figure 22. Proposed metabolism of UPCDC-10205 to the conjugated N-glucuronide

3.4.1.2 *In vitro* Metabolism

Microsome incubation samples were analyzed twice. First using the qualitative SRM LC-MS assay (2.5.2) and again to measure UPCDC-10205 using the quantitative assay (2.4.2).

The SRM method monitoring the 613 *m/z* channel revealed increasing analyte/IS ratios at the 43.6 RT. A representative chromatogram from the 60 min incubation sample is shown in Figure 23. No 43.6 min peaks were detected in any 0 min or negative control samples. The generation of metabolite over the 60 min incubation can be seen in Figure 24. The 43.6 min peak also contained 437 *m/z* trace, indicating in-source fragmentation. The rate of metabolite formation is 0.068 response ratio/min/0.25 mg protein

Measured concentrations of UPCDC-10205 divided by the time 0 concentration from the same incubation mixture were used to give a percentage of the starting amount. On average, only 67% was remaining after the incubation (Figure 24).

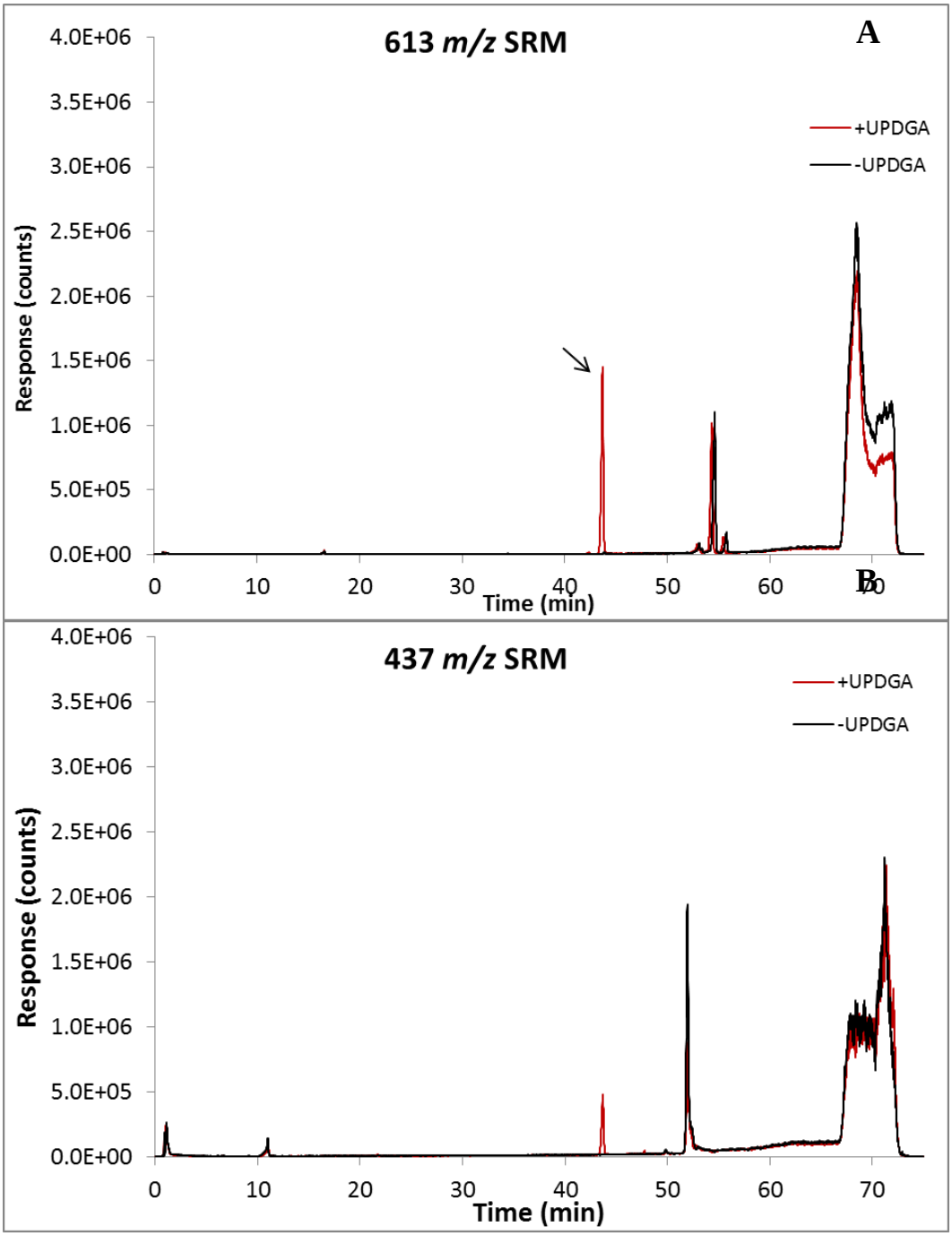

Figure 23. SRM analysis from the permeabilized microsome incubation samples, with and without UPDGA cofactor. A) 613 *m/z* channel B) 437 *m/z* channel.

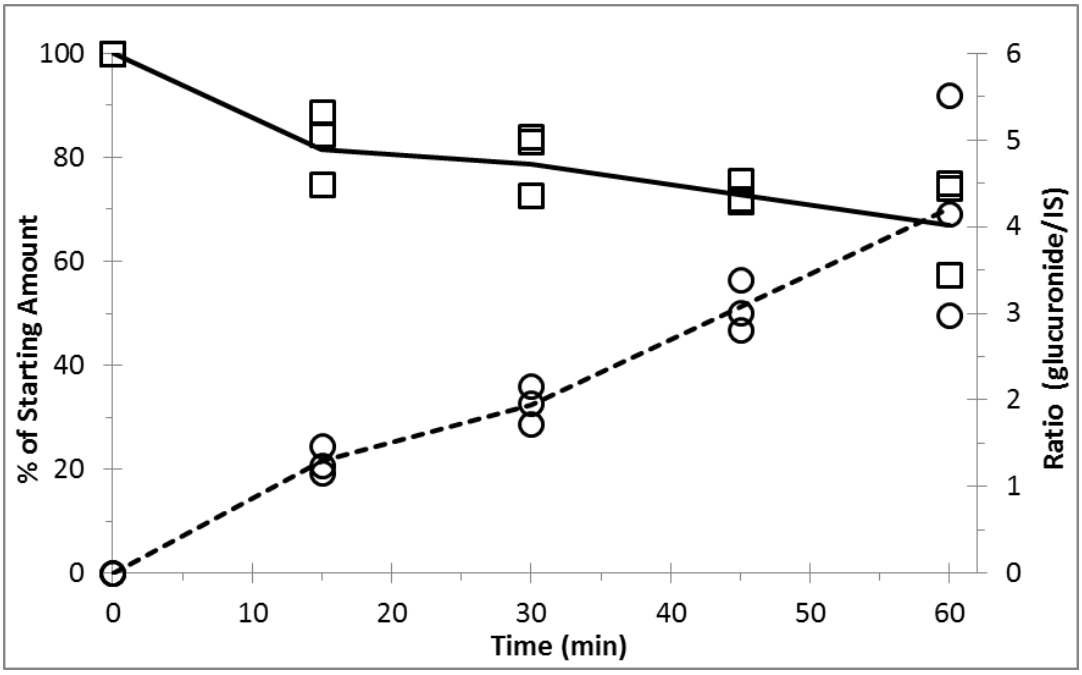

Figure 24. Microsome incubation with UPCDC-10205 with alamethicin and UPDGA to produce direct N-glucuronide (613 *m/z*). Left axis shows quantification of UPCDC-10205 (□) represented by a percent of the starting amount. Right axis shows production of metabolites (○) represented as the ratio of analyte to internal standard values.

4.0 DISCUSSION

The current standard of care for HNSCC has had little improvement on 5 year survival rates for patient's suffering from the disease, especially for those with late stage, metastatic or recurrent HNSCC. The oncogene STAT3 has been found to be constitutively active in most cancer types including HNSCC.[1, 6-8] While EGFR signaling is responsible for a portion of STAT3 activation, IL-6 signaling has been found to play a large role in the constitutive activation of STAT3, especially within the scope of HNSCC. To improve this outlook, newer therapies are being developed such as those that target IL-6 induced pSTAT3 like an mAb for IL-6 and STAT3 decoy oligonucleotides.[16, 38] To date, no small molecule inhibitors of IL-6 induced STAT3 activation have been developed. The long-term goal of our pursuit was to support the development of a small molecule to inhibit IL-6 induced of STAT3 activation that also preserves STAT1 tumor suppressive functionality. Four analogues from the 669 series of triazolothiadiazines were selected from a high-throughput screen based on meeting these criteria. Mouse liver microsomes were used because this study was a proof of principle to establish preclinical efficacy of STAT3 inhibition, and we therefore set the goal to optimize metabolic stability for this preclinical species. Human microsomes would be used as a confirmation later in the drug development process. The initial liver microsome incubation of the four analogues revealed that compound UPCDC-10205 was the most metabolically stable in the presence of phase 1 metabolizing enzymes, with approximately 80% of the compound remaining after a 90

min incubation. Based on this evidence, UPCDC-10205 was prioritized to be investigated *in vivo* to determine toxicity and PK. UPCDC-10205 demonstrated efficacy in inhibiting pSTAT3 from IL-6 induction *in vitro* using HNSCC cell lines with an IC_{50} of 2.1 µM and an IC_{100} of 4.0 µM.

Both single and multiple dose UPCDC-10205 administrations to mice demonstrated no signs of toxicity. No changes in body weight, signs of decline in clinical health, or indications of gross pathology upon necropsy were observed in either toxicity study. The lack of toxicity may very well be due to the maximum soluble concentrations of UPCDC-10205, which limited the explored dose to 4 mg/kg or less (0.4 mg/mL in 10% Solutol™ HS). Other formulations were unable to achieve higher concentrations.

Pharmacokinetics

Poor PK properties of new chemical entities are a major reason they fail during drug development.[39] Describing PK parameters can help investigators evaluate whether the new compound can potentially reach its intended target of action for long enough duration and at an appropriate concentration to achieve its intended effect as well as describing the *in vivo* fate of the drug. In these studies, we successfully determined the absorption, distribution, metabolism and elimination while simultaneously examining the potential of using UPCDC-10205 as an oral agent.

Absorption

Comparison of IV and PO dosage forms revealed UPCDC-10205 to be poorly bioavailable (5.2%) from a solution. Major factors limiting drug absorption are permeability across the epithelial lining of the GI tract, tissue binding, the first pass effect, dissolution and degradation in the gut. Furthermore, transporters can play a role in decreased absorption and

bioavailability. PgP is also known to decrease the bioavailability of a variety of different anti-cancer drugs.[40]

The first pass effect may limit bioavailability of UPCDC-10205. Absorptive transport through the hepatic portal vein allows liver exposure of UPCDC-10205 to hepatocytes containing UPDG enzymes. Biotransformation to the glucuronide prior to systemic exposure would contribute to the observed low bioavailability.

The permeability of UPCDC-10205 does not seem to impede absorption as seen in its rapid and extensive distribution observed as exposure in tissues compared to plasma. PK analysis shows slower tissue elimination than plasma elimination, which may be attributable to compound binding to lipids or protein in tissues. Corroborating this indication, tissue exposure in relation to plasma exposure shows PO dosing resulted in elevated UPCDC-10205 exposure in liver and lungs compared to IV administered mice. Orally administered drugs must pass these two organs prior to systemic distribution and can limit the bioavailability by exposing them to metabolism and biliary excretion.

High tissue binding in peripheral compartments that must be traversed prior to systemic exposure can partially explain the low bioavailability. Systemic availability of the drug could be limited in this capacity as only drug not bound to tissue is available for further distribution. Quantification of drug concentrations in tissues does not discriminate between bound and unbound. Thus, levels reported may indicate high exposure but in reality the unbound fraction available for distribution may be extremely limited by binding.

It is likely that dissolution negatively affected the bioavailability (0.34%) of the 30 mg/kg UPCDC-10205 suspension in 1% CMC. This is an example of flip-flop pharmacokinetics where

the rate of absorption is slower than the rate of elimination and the rate of absorption becomes rate-limiting to elimination, resulting in an artificially increased half-life.[41]

Distribution

The V_d observed was high, as determined by plasma analysis, and is corroborated by exposure of UPCDC-10205 observed in tissues. Highly perfused tissues, such as kidney, had 3 times the exposure compared to plasma. The T_{max} for kidneys was the same as plasma (5 minutes), indicating rapid distribution. Skeletal muscle, which is poorly perfused, had an approximately 50% increased exposure compared with plasma and had an increased T_{max} of 15 minutes. Brain exposure was similar to skeletal muscle, and demonstrates the ability of UPCDC-10205 to traverse the blood brain barrier. Analysis of RBCs did not indicate high levels of RBC drug uptake that could contribute to the observed volume of distribution. Plasma protein binding can increase V_d and limit the free fraction available for distribution.[42] The 99.9% plasma protein binding of UPCDC-10205 must contribute to the V_d but did not majorly limit distribution, as most tissue exposure was higher than plasma and this highlights the permeability of UPCDC-10205. Tissue binding may also contribute to V_d but was not investigated.

Metabolism

The first liver microsome stability study was used as a relative measure to prioritize one of the 669 series analogues by selecting against susceptibility to oxidative biotransformation. *In vivo* administration yielded a higher clearance and shorter half-life than anticipated. Identification of the direct-glucuronide metabolite as the only identified biotransformation validates the results of the original microsome incubation. It produced translatable results in that no major oxidative metabolites were identified *in vivo*. While translatable, the incubation did not allow for examination of phase II metabolic pathways as phase I are generally the rate limiting

step. The generation of the direct glucuronide metabolite *in vivo* may also contribute to the low bioavailability due to the first pass effect.

Screening for metabolites in urine and plasma proved arduous due to the presence of the vehicle. Solutol™ HS15 is an emulsifying agent consisting of mono- and disesters of 12-hydroxystearic acid and free polyethyleneglycol that are extensively hydrolyzed *in vivo*.[43] The vehicle appeared at many mass ranges and may have masked potential metabolites during MS scans. Solutol™ HS15 is known to contain 613 *m/z* traces, [43] but the unique 613 *m/z* trace from the 43.6 min peak in treated mice indicates a true metabolite. This was confirmed *in vitro* where no Solutol™ HS15 was present. While the *in vitro* glucuronidation experiment revealed 67% substrate depletion, this number may be composed of other unknown biotransformations that took place without the addition of necessary cofactors.

Elimination

Elimination is a combination of both metabolism and excretion. Excretion is largely accomplished by the kidneys and liver (via biliary secretion). Renal excretion is a combination of glomerular filtration, active secretion, and reabsorption. The size of UPCDC-10205 should permit glomerular filtration based on its MW of 436 a.m.u. This is below the glomerular threshold so the compound should freely be filtered into the renal tubule. The lipophilic nature of UPCDC-10205 also make it a likely candidate for rapid reabsorption from the lumen back into the blood stream. Despite the fact that kidneys had high exposure to UPCDC-10205, urine analysis revealed negligible UPCDC-10205 in urine demonstrating that renal excretion is not a major contributor to clearance. Because renal excretion was minimal, metabolism was thought to play a major role in elimination. The low urine amounts of UPCDC-10205 could also be attributed to high plasma protein binding as only free drug is able to be renally filtered.

The glucuronide metabolite is also below the renal threshold (612 a.m.u) but was present in urine. The presence of metabolite and not the parent in urine is most likely attributable to the increased polarity that the glucuronide adds that would prevent reabsorption. The metabolite is most likely less protein bound as well, meaning more free metabolite is available for renal and biliary excretion.

It is possible that biliary excretion of UPCDC-10205, in both its parent and metabolic forms, contributes to its elimination. Reported molecular weight cutoffs for biliary excretion vary between species, with the cutoff in rats being around 250 and humans being between 500 and 600, although more recent reports suggest that there is no clear threshold.[44, 45] The molecular weight of UPCDC-10205 falls above the threshold for rats, meaning it is susceptible to biliary excretion. It is slightly below threshold for humans, which could allow for less biliary excretion of UPCDC-10205 and increased half-life comparted to rodents. These cutoffs also apply to the metabolite, which is above the thresholds of both species, making it a likely candidate for biliary excretion as well. Biliary excretion may also contribute to low bioavailability, with drug absorbed being eliminated unchanged. Reabsorption after biliary excretion is unlikely to have a significant effect based on the observed bioavailability.

Metabolic stability is important in selecting a successful drug candidate.[46, 47] It is also important to analyze *in vitro* metabolic stability if oral use is a goal of candidate selection because presystemic metabolism can limit bioavailability.[48] Choosing a candidate based on metabolic stability, instead solely on *in vitro* potency, often yields more efficacious leads.[49, 50] *In vitro* metabolic stability is used a predictor for *in vivo* metabolic clearance.[46] Prioritization of UPCDC-10205 was based on metabolic stability conveyed from the initial microsome incubation

but only accounted for phase I metabolism with the rationale that cyp P450s account for the metabolism for about 90% of all drugs.[46, 48]

There are many reasons to prioritize the use of microsomes. Besides practical aspects of cost and complexity, these include the ideas that cytochrome P450 metabolism is usually rate limiting steps in biotransformation and cytochrome P450 metabolism is the major ADME reason for drug failure during development.[48] The major disadvantage for using microsome screens as a measure of metabolic stability is that they do not represent the complete *in vivo* system of metabolizing enzymes and only have the capacity to stably represent CYPs and UGTs. The promotion of a compound from the 669 series was designed as a relative measure of metabolic stability due to cytochrome P450s being the major factor in metabolism of drugs.[46]

Prioritization could have been accomplished using hepatocytes or liver slices to accommodate all forms of enzymatic biotransformation. While these methods are more representative of human metabolism they can have disadvantages such as having reduced enzymatic activity by lacking sufficient cofactor production in cells.[51, 52] Direct glucuronidation, as identified with UPCDC-10205, does not require prior phase I metabolic biotransformation.[52] The 20% substrate depletion of UPCDC-10205 observed in the initial lead selection incubation did not account for glucuronidation. The incubation conducted to produce the glucuronide depleted approximately 25% of UPCDC-10205 in 60 minutes, which demonstrates its susceptibility to direct conjugation.

Two other analogues from the 669 series contain the pyrazole groups postulated as the site for direct glucuronidation making it possible they may also experience the observed direct glucuronidation. UPCDC-10540 has a methyl group attached to the pyrazole which may prevent susceptibility to N-glucuronidation. UPCDC-10540, UPCDC-10305 and 864669 would likely

experience more extensive metabolism than UPCDC-10205 due to their higher levels of phase I metabolism observed *in vitro*. These phase I metabolites may also increase the metabolic contribution to clearance as well their potential for non-direct glucuronidation.

Pyrazole groups are a common motif used in small molecule drugs. The available electron pair on either nitrogen of the pyrazole group is able to be targeted by UGTs for conjugation. N-glucuronidation is largely accomplished through UGT isoforms 1A4 and 2B10 and the enzyme amounts of these isoforms is higher in humans than other animals.[53] These enzymes exist primarily in the liver, but UGT1A4 expression has also been detected in kidneys, and may also contribute to metabolic clearance.[54] Glucuronidation can also occur in intestinal microsomes, which could also to contribute to decreased bioavailability.[55] Extrahepatic glucuronidation can contribute to the clearance observed in the PK studies, especially in orally delivered UPCDC-10205. Other compounds subjected to direct N-glucuronidation by UGT 2B10 include tertiary or cyclic amines.[56] Scaling of the *in vivo* or *in vitro* glucuronidation results to humans seems unpredictable as both UGT2B10 and 1A4 exhibit high levels of variability in expression from analysis on human liver samples.[57] UGT2B10 appears to have a higher affinity for tertiary and cyclic amines than UGT 1A4 but expression amounts in the liver are not equal.[56] Extrapolation of metabolic rates to human appears difficult due to species variability of glucuronidation rates.[58] Additionally, the scaling of *in vitro* glucuronidation rates to *in vivo* generally underestimates clearance due to glucuronidation.[59] Direct N-glucuronidation to pyrazole groups of small molecule drugs has been observed previously.[60-63]

Other compounds undergoing extensive N-glucuronidation on pyrazole groups have been optimized to add substituents to the pyrazole in order to decrease susceptibility to direct glucuronidation.[63] Molecular addition of electronegative groups may reduce nucleophilic

tendencies of pyrazole nitrogens and decrease availability for direct glucuronidation. This method has been explored with other pyrazole containing small molecules that underwent rapid N-glucuronidation.[64] Alterations to UPCDC-10205 could potentially increase bioavailability and decrease metabolic clearance.

5.0 CONCLUSIONS AND FUTURE DIRECTIONS

The aim of this project was to prioritize an IL-6 induced STAT3 inhibitor that was selective for STAT3 and to describe the toxicology, PK and metabolism of the compound. UPCDC-10205 was prioritized for *in vivo* administration to determine if the compound deserves further preclinical investigation. While UPCDC-10205 demonstrated *in vitro* potency and selectivity, several factors were identified *in vivo* that limit UPCDC-10205's potential as a future clinical therapeutic. Preclinical pharmacokinetics create a bottleneck for anticancer drug development, so prioritization and evidence gathering on PK is of importance. Solubility, metabolism, and plasma protein binding have been identified through these studies as the major limiting factors of UPCDC-10205's potential. PK and bioavailability are the 3rd most common cause of drug development attrition.[39] While the percentage of drugs whose attrition is related to DMPK has been lowered over the last 30 years, it still accounts for approximately 11% of drug failures.[65]

Future investigations for the development of small molecule inhibitors of IL-6 induced pSTAT3 should investigate the structure activity relationship (SAR) of the 669 analogue series with the IL-6/STAT3 signaling cascade. An SAR may allow elucidation of active chemical epitopes and potentially help reduce future metabolic lability, decrease protein binding, and increase solubility while simultaneously maintaining potency and selectivity.

BIBLIOGRAPHY

1. Argiris A. EGFR inhibition for recurrent or metastatic HNSCC. The Lancet Oncology. 2015;16(5):488-9.
2. Murata M, Takayama K, Choi BC, Pak AW. A nested case-control study on alcohol drinking, tobacco smoking, and cancer. Cancer detection and prevention. 1996;20(6):557-65.
3. Paz IB, Cook N, Odom-Maryon T, Xie Y, Wilczynski SP. Human papillomavirus (HPV) in head and neck cancer. An association of HPV 16 with squamous cell carcinoma of Waldeyer's tonsillar ring. Cancer. 1997;79(3):595-604.
4. Siegel RL, Miller KD, Jemal A, Yu H, Lee H, Herrmann A, et al. Cancer statistics, 2015. CA Cancer J Clin. 2015;65(1):5-29.
5. Sacco AG, Cohen EE, Waring MJ, Arrowsmith J, Leach AR, Leeson PD, et al. Current Treatment Options for Recurrent or Metastatic Head and Neck Squamous Cell Carcinoma. J Clin Oncol. 2015;33(29):3305-13.
6. Geiger JL, Grandis JR, Bauman JE. The STAT3 pathway as a therapeutic target in head and neck cancer: Barriers and innovations. Oral Oncol. 2016;56:84-92.
7. Argiris A, Karamouzis MV, Raben D, Ferris RL. Head and neck cancer. Lancet (London, England). 2008;371(9625):1695-709.
8. Frank DA. STAT3 as a central mediator of neoplastic cellular transformation. Cancer letters. 2007;251(2):199-210.
9. Wang X, Crowe PJ, Goldstein D, Yang JL. STAT3 inhibition, a novel approach to enhancing targeted therapy in human cancers (review). International journal of oncology. 2012;41(4):1181-91.
10. Sriuranpong V, Park JI, Amornphimoltham P, Patel V, Nelkin BD, Gutkind JS. Epidermal growth factor receptor-independent constitutive activation of STAT3 in head and neck squamous cell carcinoma is mediated by the autocrine/paracrine stimulation of the interleukin 6/gp130 cytokine system. Cancer research. 2003;63(11):2948-56.
11. Sen M, Joyce S, Panahandeh M, Li C, Thomas SM, Maxwell J, et al. Targeting Stat3 abrogates EGFR inhibitor resistance in cancer. Clinical cancer research : an official journal of the American Association for Cancer Research. 2012;18(18):4986-96.
12. Aggarwal BB, Kunnumakkara AB, Harikumar KB, Gupta SR, Tharakan ST, Koca C, et al. Signal transducer and activator of transcription-3, inflammation, and cancer: how intimate is the relationship? Annals of the New York Academy of Sciences. 2009;1171:59-76.
13. Yu H, Lee H, Herrmann A, Buettner R, Jove R. Revisiting STAT3 signalling in cancer: new and unexpected biological functions. Nature reviews Cancer. 2014;14(11):736-46.

14. Spitzner M, Ebner R, Wolff HA, Ghadimi BM, Wienands J, Grade M. STAT3: A Novel Molecular Mediator of Resistance to Chemoradiotherapy. Cancers. 2014;6(4):1986-2011.
15. Bromberg JF, Wrzeszczynska MH, Devgan G, Zhao Y, Pestell RG, Albanese C, et al. Stat3 as an oncogene. Cell. 1999;98(3):295-303.
16. Johnston PA, Grandis JR. STAT3 signaling: anticancer strategies and challenges. Mol Interv. 2011;11(1):18-26.
17. Haura EB, Turkson J, Jove R. Mechanisms of disease: Insights into the emerging role of signal transducers and activators of transcription in cancer. Nature clinical practice Oncology. 2005;2(6):315-24.
18. Niu G, Wright KL, Huang M, Song L, Haura E, Turkson J, et al. Constitutive Stat3 activity up-regulates VEGF expression and tumor angiogenesis. Oncogene. 2002;21(13):2000-8.
19. Hodge DR, Hurt EM, Farrar WL. The role of IL-6 and STAT3 in inflammation and cancer. European journal of cancer (Oxford, England : 1990). 2005;41(16):2502-12.
20. Riedel F, Zaiss I, Herzog D, Gotte K, Naim R, Hormann K. Serum levels of interleukin-6 in patients with primary head and neck squamous cell carcinoma. Anticancer research. 2005;25(4):2761-5.
21. Duffy SA, Taylor JM, Terrell JE, Islam M, Li Y, Fowler KE, et al. Interleukin-6 predicts recurrence and survival among head and neck cancer patients. Cancer. 2008;113(4):750-7.
22. De Schutter H, Landuyt W, Verbeken E, Goethals L, Hermans R, Nuyts S. The prognostic value of the hypoxia markers CA IX and GLUT 1 and the cytokines VEGF and IL 6 in head and neck squamous cell carcinoma treated by radiotherapy +/- chemotherapy. BMC cancer. 2005;5:42.
23. Wang SW, Sun YM. The IL-6/JAK/STAT3 pathway: potential therapeutic strategies in treating colorectal cancer (Review). International journal of oncology. 2014;44(4):1032-40.
24. Safdari Y, Khalili M, Farajnia S, Asgharzadeh M, Yazdani Y, Sadeghi M. Recent advances in head and neck squamous cell carcinoma--a review. Clinical biochemistry. 2014;47(13-14):1195-202.
25. Hennigan S, Kavanaugh A. Interleukin-6 inhibitors in the treatment of rheumatoid arthritis. Therapeutics and clinical risk management. 2008;4(4):767-75.
26. Yue P, Turkson J. Targeting STAT3 in cancer: how successful are we? Expert Opin Investig Drugs. 2009;18(1):45-56.
27. Oh DY, Lee SH, Han SW, Kim MJ, Kim TM, Kim TY, et al. Phase I Study of OPB-31121, an Oral STAT3 Inhibitor, in Patients with Advanced Solid Tumors. Cancer research and treatment : official journal of Korean Cancer Association. 2015;47(4):607-15.
28. Avalle L, Pensa S, Regis G, Novelli F, Poli V. STAT1 and STAT3 in tumorigenesis: A matter of balance. Jakstat. 2012;1(2):65-72.
29. Szelag M, Czerwoniec A, Wesoly J, Bluyssen HA. Identification of STAT1 and STAT3 specific inhibitors using comparative virtual screening and docking validation. PLoS One. 2015;10(2):e0116688.
30. Bromberg J. Stat proteins and oncogenesis. The Journal of clinical investigation. 2002;109(9):1139-42.

31. Regis G, Pensa S, Boselli D, Novelli F, Poli V, Duffy SA, et al. Ups and downs: the STAT1:STAT3 seesaw of Interferon and gp130 receptor signalling. Semin Cell Dev Biol. 2008;19(4):351-9.
32. Johnston PA, Sen M, Hua Y, Camarco D, Shun TY, Lazo JS, et al. High-content pSTAT3/1 imaging assays to screen for selective inhibitors of STAT3 pathway activation in head and neck cancer cell lines. Assay and drug development technologies. 2014;12(1):55-79.
33. Johnston PA, Sen M, Hua Y, Camarco DP, Shun TY, Lazo JS, et al. HCS campaign to identify selective inhibitors of IL-6-induced STAT3 pathway activation in head and neck cancer cell lines. Assay and drug development technologies. 2015;13(7):356-76.
34. Hefti FF. Requirements for a lead compound to become a clinical candidate. BMC Neurosci. 2008;9 Suppl 3:S7.
35. Jia L, Liu X. The conduct of drug metabolism studies considered good practice (II): in vitro experiments. Current drug metabolism. 2007;8(8):822-9.
36. Hill JR. In vitro drug metabolism using liver microsomes. Current protocols in pharmacology / editorial board, SJ Enna (editor-in-chief) [et al]. 2004;Chapter 7:Unit7 8.
37. Seo KA, Kim HJ, Jeong ES, Abdalla N, Choi CS, Kim DH, et al. In vitro assay of six UDP-glucuronosyltransferase isoforms in human liver microsomes, using cocktails of probe substrates and liquid chromatography-tandem mass spectrometry. Drug Metab Dispos. 2014;42(11):1803-10.
38. Fagard R, Metelev V, Souissi I, Baran-Marszak F. STAT3 inhibitors for cancer therapy: Have all roads been explored? Jakstat. 2013;2(1):e22882.
39. Waring MJ, Arrowsmith J, Leach AR, Leeson PD, Mandrell S, Owen RM, et al. An analysis of the attrition of drug candidates from four major pharmaceutical companies. Nature reviews Drug discovery. 2015;14(7):475-86.
40. Schellens JH, Malingre MM, Kruijtzer CM, Bardelmeijer HA, van Tellingen O, Schinkel AH, et al. Modulation of oral bioavailability of anticancer drugs: from mouse to man. European journal of pharmaceutical sciences : official journal of the European Federation for Pharmaceutical Sciences. 2000;12(2):103-10.
41. Yanez JA, Remsberg CM, Sayre CL, Forrest ML, Davies NM. Flip-flop pharmacokinetics--delivering a reversal of disposition: challenges and opportunities during drug development. Therapeutic delivery. 2011;2(5):643-72.
42. Ye M, Nagar S, Korzekwa K. A physiologically based pharmacokinetic model to predict the pharmacokinetics of highly protein-bound drugs and the impact of errors in plasma protein binding. Biopharmaceutics & drug disposition. 2016;37(3):123-41.
43. Bhaskar VV, Middha A, Srivastava P, Rajagopal S. Liquid chromatography/tandem mass spectrometry method for quantitative estimation of solutol HS15 and its applications. Journal of Pharmaceutical Analysis. 2015;5(2):120-9.
44. Yang X, Gandhi YA, Duignan DB, Morris ME. Prediction of biliary excretion in rats and humans using molecular weight and quantitative structure-pharmacokinetic relationships. The AAPS journal. 2009;11(3):511-25.
45. Ghibellini G, Leslie EM, Brouwer KL. Methods to evaluate biliary excretion of drugs in humans: an updated review. Molecular pharmaceutics. 2006;3(3):198-211.
46. Pelkonen O, Turpeinen M, Uusitalo J, Rautio A, Raunio H. Prediction of drug metabolism and interactions on the basis of in vitro investigations. Basic Clin Pharmacol Toxicol. 2005;96(3):167-75.

47. Obach RS, Baxter JG, Liston TE, Silber BM, Jones BC, MacIntyre F, et al. The prediction of human pharmacokinetic parameters from preclinical and in vitro metabolism data. The Journal of pharmacology and experimental therapeutics. 1997;283(1):46-58.
48. Cayen MN. Early Drug Development: Strategies and Routes to First-in-Human Trials. Hoboken, N.J: Wiley; 2010.
49. Gleeson MP, Hersey A, Montanari D, Overington J. Probing the links between in vitro potency, ADMET and physicochemical parameters. Nature reviews Drug discovery. 2011;10(3):197-208.
50. Horst W. Doelle JSR, Marin Berovic. BIOTECHNOLOGY: Fundamentals in Biotechnology: Encyclopedia of Life Support Systems; 2009.
51. Borchardt RT SP, Wilson G. Models for Assessing Drug Absorption and Metabolism. 1 ed. New York, NY: Springer US; 1996. 444 p.
52. Brandon EF, Raap CD, Meijerman I, Beijnen JH, Schellens JH. An update on in vitro test methods in human hepatic drug biotransformation research: pros and cons. Toxicology and applied pharmacology. 2003;189(3):233-46.
53. Kaivosaari S, Finel M, Koskinen M. N-glucuronidation of drugs and other xenobiotics by human and animal UDP-glucuronosyltransferases. Xenobiotica. 2011;41(8):652-69.
54. Harbourt DE, Fallon JK, Ito S, Baba T, Ritter JK, Glish GL, et al. Quantification of human uridine-diphosphate glucuronosyl transferase 1A isoforms in liver, intestine, and kidney using nanobore liquid chromatography-tandem mass spectrometry. Anal Chem. 2012;84(1):98-105.
55. Fisher MB, Paine MF, Strelevitz TJ, Wrighton SA. The role of hepatic and extrahepatic UDP-glucuronosyltransferases in human drug metabolism. Drug metabolism reviews. 2001;33(3-4):273-97.
56. Kato Y, Izukawa T, Oda S, Fukami T, Finel M, Yokoi T, et al. Human UDP-glucuronosyltransferase (UGT) 2B10 in drug N-glucuronidation: substrate screening and comparison with UGT1A3 and UGT1A4. Drug Metab Dispos. 2013;41(7):1389-97.
57. Izukawa T, Nakajima M, Fujiwara R, Yamanaka H, Fukami T, Takamiya M, et al. Quantitative analysis of UDP-glucuronosyltransferase (UGT) 1A and UGT2B expression levels in human livers. Drug Metab Dispos. 2009;37(8):1759-68.
58. Chiu SH, Huskey SW. Species differences in N-glucuronidation. Drug Metab Dispos. 1998;26(9):838-47.
59. Miners JO, Smith PA, Sorich MJ, McKinnon RA, Mackenzie PI. Predicting human drug glucuronidation parameters: application of in vitro and in silico modeling approaches. Annual review of pharmacology and toxicology. 2004;44:1-25.
60. Yan Z, Caldwell GW, Gauthier D, Leo GC, Mei J, Ho CY, et al. N-glucuronidation of the platelet-derived growth factor receptor tyrosine kinase inhibitor 6,7-(dimethoxy-2,4-dihydroindeno[1,2-C]pyrazol-3-yl)-(3-fluoro-phenyl)-amine by human UDP-glucuronosyltransferases. Drug Metab Dispos. 2006;34(5):748-55.
61. Vourvahis M, Gleave M, Nedderman AN, Hyland R, Gardner I, Howard M, et al. Excretion and metabolism of lersivirine (5-{[3,5-diethyl-1-(2-hydroxyethyl)(3,5-14C2)-1H-pyrazol-4-yl]oxy}benzene-1,3-dic arbonitrile), a next-generation non-nucleoside reverse transcriptase inhibitor, after administration of [14C]Lersivirine to healthy volunteers. Drug Metab Dispos. 2010;38(5):789-800.

62. Peterson EA, Boezio AA, Andrews PS, Boezio CM, Bush TL, Cheng AC, et al. Discovery and optimization of potent and selective imidazopyridine and imidazopyridazine mTOR inhibitors. Bioorg Med Chem Lett. 2012;22(15):4967-74.
63. Dressen D, Garofalo AW, Hawkinson J, Hom D, Jagodzinski J, Marugg JL, et al. Preparation and optimization of a series of 3-carboxamido-5-phenacylaminopyrazole bradykinin B1 receptor antagonists. J Med Chem. 2007;50(21):5161-7.
64. Ye XM, Konradi AW, Smith J, Aubele DL, Garofalo AW, Marugg J, et al. Discovery of a novel sulfonamide-pyrazolopiperidine series as potent and efficacious gamma-secretase inhibitors (Part II). Bioorg Med Chem Lett. 2010;20(12):3502-6.
65. Khanna I. Drug discovery in pharmaceutical industry: productivity challenges and trends. Drug discovery today. 2012;17(19-20):1088-102.